Q. J. R. Meteorol. Soc. (1999), **125**, pp. 941–965

The role of vertically varying cloud fraction in the parametrization of microphysical processes in the ECMWF model

By CHRISTIAN JAKOB[1]* and STEPHEN A. KLEIN[2]
[1]*European Centre for Medium-Range Weather Forecasts, UK*
[2]*Geophysical Fluid Dynamics Laboratory/NOAA, USA*

(Received 17 March 1998; revised 20 July 1998)

SUMMARY

General-circulation models (GCMs) have generally treated solely the radiative impacts of vertically varying cloud fraction by using a cloud-overlap assumption. In this study, the microphysical impacts of vertically varying cloud fraction are addressed by developing a subgrid-scale precipitation model which resolves the vertical variation of cloud fraction. This subgrid model subdivides the grid boxes into homogeneous columns which are either clear or completely cloudy. By comparing the column-averaged microphysical quantities from the subgrid-scale precipitation model with the parametrization in the European Centre for Medium-Range Forecasts (ECMWF) model, the ability of the ECMWF model to account for the subgrid nature of cloud and precipitation microphysics is assessed. It is found that the ECMWF model overestimates the evaporation of precipitation in the tropical mid-troposphere. This results from (a) an incorrect parametrization of the area of the grid box covered by precipitation, and (b) the inadequacy of assuming a single value for the precipitation rate in the grid box.

In addition to assessing the ability of the ECMWF model to parametrize the subgrid nature of cloud microphysics, the subgrid precipitation model is used to show that the cloud-overlap assumption has a large impact on the evaporation of precipitation. In light of the current trend towards more sophisticated cloud and precipitation parametrizations in GCMs, more attention should be paid to the impact of vertical cloud-fraction variations on the parametrized microphysics.

KEYWORDS: Global-circulation model Precipitation Subgrid-scale variability

1. INTRODUCTION

The representation of clouds in atmospheric general-circulation models (GCMs) has evolved considerably over the last ten years. Almost all global models now include parametrizations that describe the budget of the cloud condensate for each of the models' vertical levels with a prognostic equation (e.g. Sundqvist 1978; Smith 1990; Tiedtke 1993; Fowler *et al.* 1996; Del Genio *et al.* 1996). The predicted cloud condensate is then used for radiation calculations, thereby coupling the cloud radiative forcing to the latent-heat release associated with the condensation and evaporation processes.

Besides parametrizing the density of cloud condensate, many parametrizations also describe, in some form, the fraction of a GCM grid box covered by clouds (Sundqvist 1978; Smith 1990; Tiedtke 1993). Cloud-fraction parametrizations of this kind represent, in a simple way, the complex structure of cloud fields both in the horizontal and in the vertical. Figure 1 is a schematic of a distribution of clouds frequently encountered in tropical convective situations (e.g. Houze and Betts 1981) where penetrating convective towers with their associated anvils and outflow cirrus coexist with shallow or medium convective clouds. One may ask if a cloud parametrization scheme ought to resolve some of the variability shown in Fig. 1 by representing the vertically varying cloud fraction and condensate.

Vertical variations in cloud fraction and optical thickness influence the distribution of the radiative fluxes in the atmosphere. Radiation parametrization schemes account for this variability by introducing overlap assumptions (e.g. Geleyn and Hollingsworth 1979; Morcrette and Fouquart 1986) which determine the horizontal position of a 'cloud' at each model level relative to the clouds at other model levels. Yu *et al.* (1996) have used these overlap assumptions to divide model grid boxes into sub-columns when comparing model

* Corresponding author: European Centre for Medium-Range Weather Forecasts, Shinfield Park, Reading, RG2 9AX, UK.

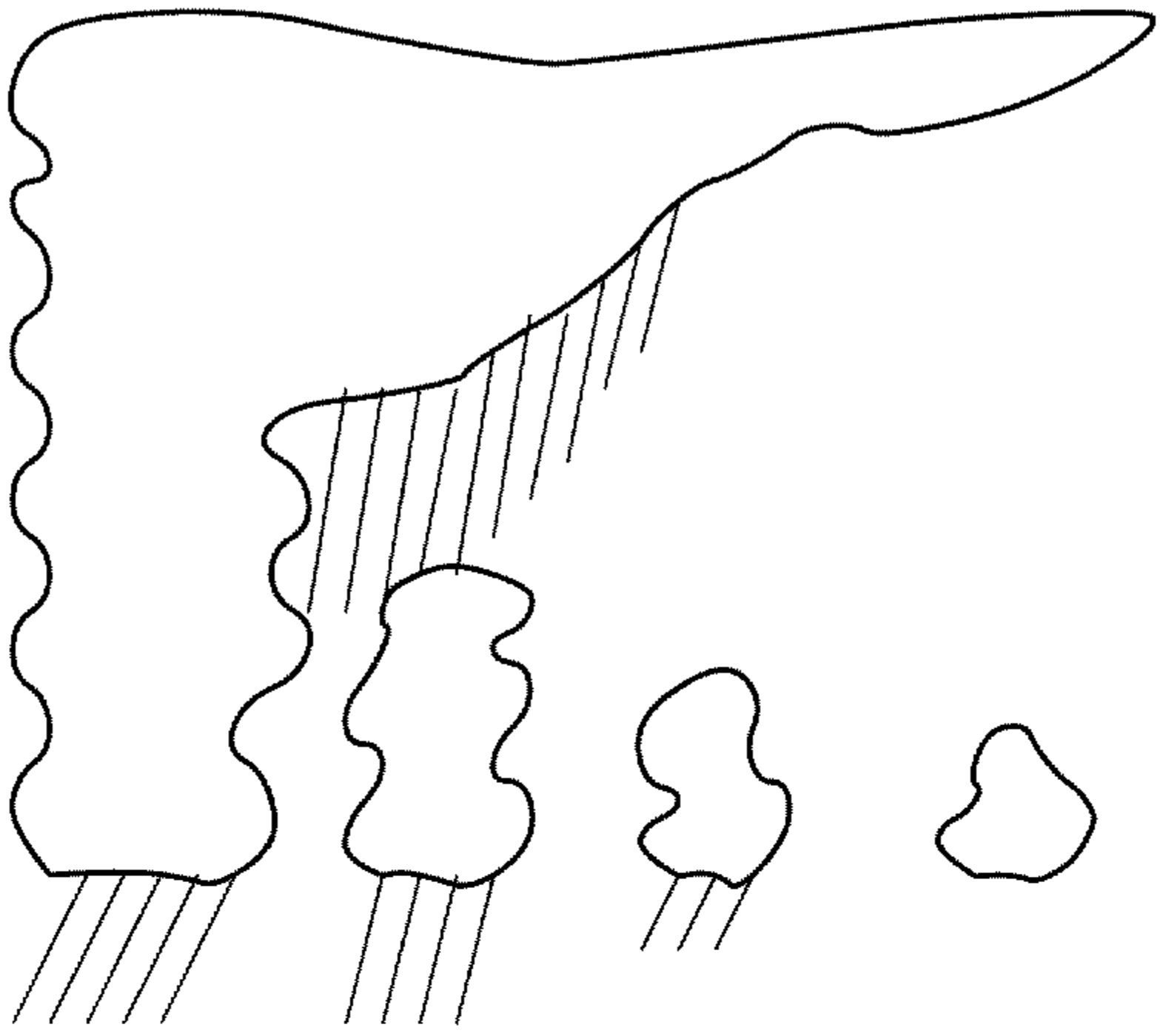

Figure 1. Schematic of a typical cloud distribution in the tropics.

clouds to satellite observations. Stubenrauch *et al.* (1997) recently proposed an overlap scheme which creates blocks of cloud spanning several model levels in the vertical, and then distributes the blocks in the horizontal following certain overlap rules.

The effects of vertical variations of cloud fraction on the parametrization of microphysical processes have received less attention than their radiative effects. For instance, if ice from a cirrus anvil falls into a cloud with supercooled liquid water (as depicted in the leftmost low cloud in Fig. 1), then the liquid water may be converted to ice through the Bergeron process (Baker 1997). Whether or not this occurs depends on whether the anvil ice falls into the lower cloud. Similarly, evaporation of precipitation can only occur when precipitation falls into clear air. GCMs have shown a large sensitivity to the treatment of the evaporation of precipitation (e.g. Gregory 1995), and it therefore appears to be desirable to treat the subgrid-scale nature of the evaporation process more carefully. A few studies have tried to account for such effects by determining a precipitation fraction (Rotstayn 1997) or by adjusting microphysical parameters, such as autoconversion rates and accretion rates in cases of vertically varying cloud (Bechtold *et al.* 1993).

This exploratory study investigates the microphysical and macrophysical impact of an explicit treatment of vertical variation of cloud fraction in the ECMWF* 1993 (E93) cloud scheme (Tiedtke 1993; Jakob 1994). The technique applied is to divide each grid box horizontally at each level into N smaller 'sub-boxes'. Each of the sub-boxes is assigned to be either clear or completely cloudy, depending both on the cloud fraction predicted for the whole grid box by the cloud parametrization and on the cloud-overlap assumption used by the radiation parametrization. This yields N vertical columns of sub-boxes with up to N different vertical distributions of cloud. The microphysics parametrization is then

* European Centre for Medium-Range Weather Forecasts

calculated separately for each column of sub-boxes. The relevant grid-mean quantities (e.g. precipitation fluxes, evaporation rates etc.) are computed by averaging over all sub-boxes. Comparison with the results of the original parametrization provides an indication of the subgrid-scale effects of cloud microphysics.

Section 2 describes the E93 parametrization and the subgrid-scale precipitation model is introduced in section 3. Section 4 compares the results from the more complex treatment with the results from the E93 parametrization, and discusses the main differences. A summary and discussion of the results is given in section 5.

2. The 1993 ECMWF cloud scheme

The E93 cloud scheme has been described in detail by Tiedtke (1993), and some later changes have been listed by Jakob (1994). The scheme is based on two prognostic equations for cloud fraction a and cloud condensate l (the sum of cloud liquid water and ice), i.e.

$$\frac{\partial a}{\partial t} = A_a + S_a - D_a, \tag{1}$$

and

$$\frac{\partial l}{\partial t} = A_l + S_l - D_l, \tag{2}$$

where A_a and A_l represent the advective terms, S_a and S_l represent the source terms, and D_a and D_l represent the dissipation terms for the cloud fraction and condensate, respectively. Sources for cloud fraction and condensate in the scheme arise from convection, boundary-layer turbulence in case of stratocumulus clouds, large-scale lifting and diabatic cooling. The dissipation terms are determined by evaporation processes due to subsiding motion (including both large-scale subsidence and cumulus-induced subsidence), diabatic heating, turbulent erosion processes at both cloud top and cloud sides, and by precipitation processes in the case of condensate.

The parametrization of microphysical processes is as described by Tiedtke (1993) and Jakob (1994) throughout this study. The generation of precipitation is dependent on the phase of the condensate, which is distinguished between pure ice, mixed-phase water and pure water by a quadratic function of temperature varying from pure ice below −23°C to pure water above 0°C. For pure-ice clouds, the mean terminal fall velocity of ice particles is prescribed as a function of ice content following Heymsfield and Donner (1990). In mixed-phase and water clouds, Sundqvist's (1988) conversion scheme is used. The evaporation of rain and snow follows the formulation of Kessler (1969) and the melting of snow is parametrized by allowing a layer to cool to the melting point (0°C) over a time-scale of five hours. The numerical treatment is implicit for the conversion from cloud water and ice to precipitation (Tiedtke 1993), and explicit for melting and evaporation.

As suggested by Fig. 1, large vertical variations in cloud fraction can exist in nature over an area the size of a GCM grid box. Before investigating whether the representation of these effects in the ECMWF model is of importance, it is necessary to establish if the model produces significant vertical variations in cloud fraction. Figure 2 shows the zonal-mean cloud distribution as a function of latitude and model level in the operational model for 12 UTC 1 July 1997. The zonal-mean cloud fraction varies substantially in the vertical. However, in the zonal mean such a variation could be caused by the occurrence of clouds at different grid points in the horizontal and does not necessarily imply strong vertical variations at any given location. However, Fig. 3 shows the cloud-fraction profile for a

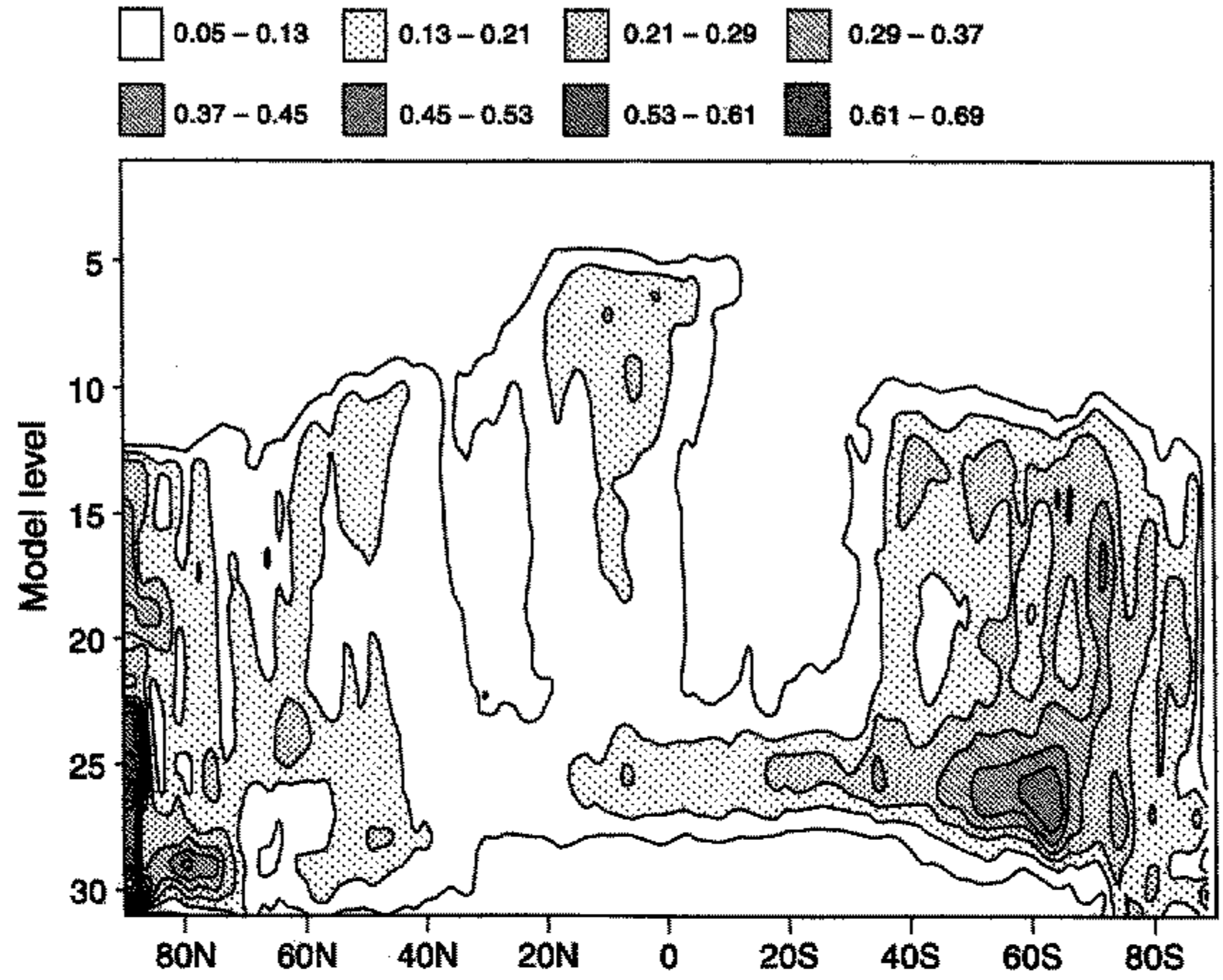

Figure 2. Zonal-mean distribution of the cloud fraction in the ECMWF model for 12 UTC 1 July 1997 as a function of latitude and model level (the model-level number decreases with pressure, as indicated in the axis labelling of Fig. 3).

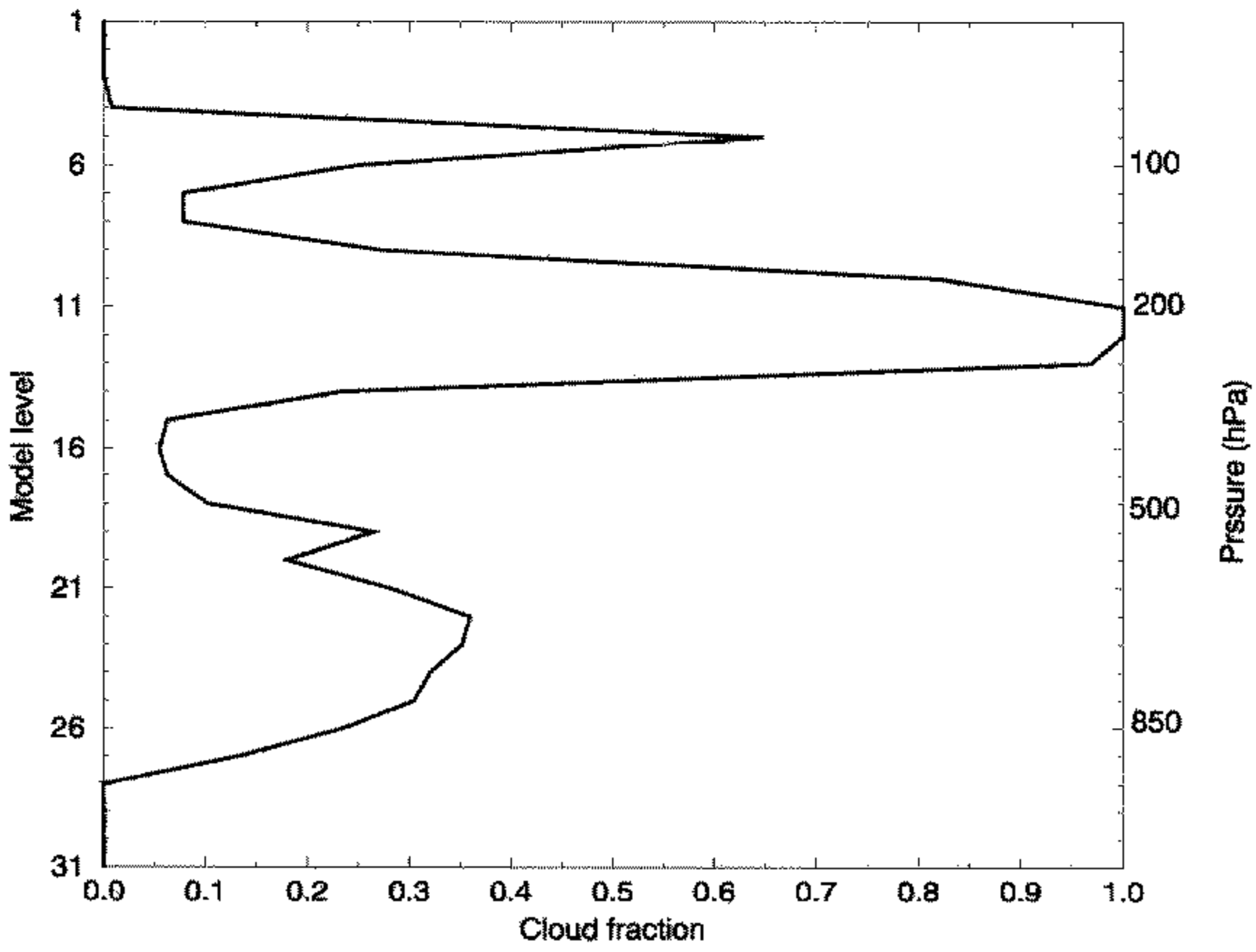

Figure 3. Vertical profile at a single point in the tropics (2°N, 160°E) of the cloud-fraction distribution illustrated in Fig. 2.

single randomly chosen point in the tropics, and it is evident that instantaneous local cloud fields produced by the ECMWF scheme can indeed have large vertical variations of cloud fraction. The cloud fields depicted in Figs. 2 and 3 form the basis of the investigations in the following sections.

3. The subgrid-scale precipitation model

Bulk microphysical parametrizations (e.g. Hsie *et al.* 1980; Lin *et al.* 1983; Rutledge and Hobbs 1983) describing the formation and evaporation of different precipitation species are typically formulated such that they are applicable on small scales in regions that are either clear or totally cloudy. Their application in large volumes, such as a GCM grid box that can contain both cloudy and cloud-free areas, is therefore not straightforward. Several approaches to this problem have been proposed. The simplest approach is to ignore partial cloudiness and assume the cloud fraction to be 1 whenever condensate occurs in a grid box (e.g. Fowler *et al.* 1996). Schemes that parametrize cloud fraction are often expressed in terms of the in-cloud water content $l_c = l/a$ in microphysical calculations, where l is the grid-mean liquid-water and ice content and a is the cloud fraction (Tiedtke 1993). Until very recently (Bechthold *et al.* 1993; Tiedtke 1993; Rotstayn 1997), parametrizations have ignored the rather obvious fact that partial cloudiness may give rise to precipitation covering only a fraction of the area of a grid box.

In order to assess the effects of partial cloudiness and partial precipitation coverage systematically, a subgrid-scale precipitation representation has been developed. The basic idea is to subdivide each grid box into N sub-columns ($N = 20$ is used for most of this study) in which the cloud fraction is assigned to be either 0 or 1 at each model level. The microphysical parametrization is then applied to each of the sub-columns and the relevant grid-mean quantities (e.g. precipitation flux, and melting and evaporation rates) are calculated by summing up the values over all sub-columns. This is equivalent to adopting an increased horizontal resolution for the microphysical calculations. A possible distribution of cloudy and clear-sky sub-columns for the distribution of cloud fraction in Fig. 3 is shown in Fig. 4. Several assumptions were made in arriving at the distribution of cloudy and clear-sky sub-columns shown, the details of which are explained below.

Firstly, it is assumed that when clouds are present they completely fill the grid box in the vertical; i.e. the fraction of grid box volume that contains cloud is equal to the fraction of the horizontal area of a grid box that contains cloud. For the ECMWF model, which has 31 levels in the vertical with typical resolution of 40 hPa (about 400 to 700 m) in the troposphere, this may not be too bad an approximation, although many clouds are observed to have thicknesses less than 500 m (Wang and Rossow 1995).

Secondly, at each level the specification of which sub-columns contain cloud is entirely consistent with the cloud-overlap assumption used for the subgrid-scale flux calculations in the radiation scheme. The overlap assumption currently used in the radiation scheme is that of maximum-random overlap (Geleyn and Hollingsworth 1979; Morcrette and Fouquart 1986). It can be described using the following equation which specifies the total horizontal area, C^k, covered by clouds between the top of the atmosphere and a given model level k as :

$$\frac{1 - C^k}{1 - C^{k-1}} = \frac{1 - \max(a^{k-1}, a^k)}{1 - \min(a^{k-1}, 1 - \delta)}, \tag{3}$$

where a^k is the cloud fraction of level k , $\delta \equiv 10^{-6}$, and $k \equiv 1$ for the top model level (C^0 and a^0 are set to zero). This equation yields random overlap for clouds which do not occur in adjacent vertical levels, but maximum overlap if clouds occur at adjacent levels

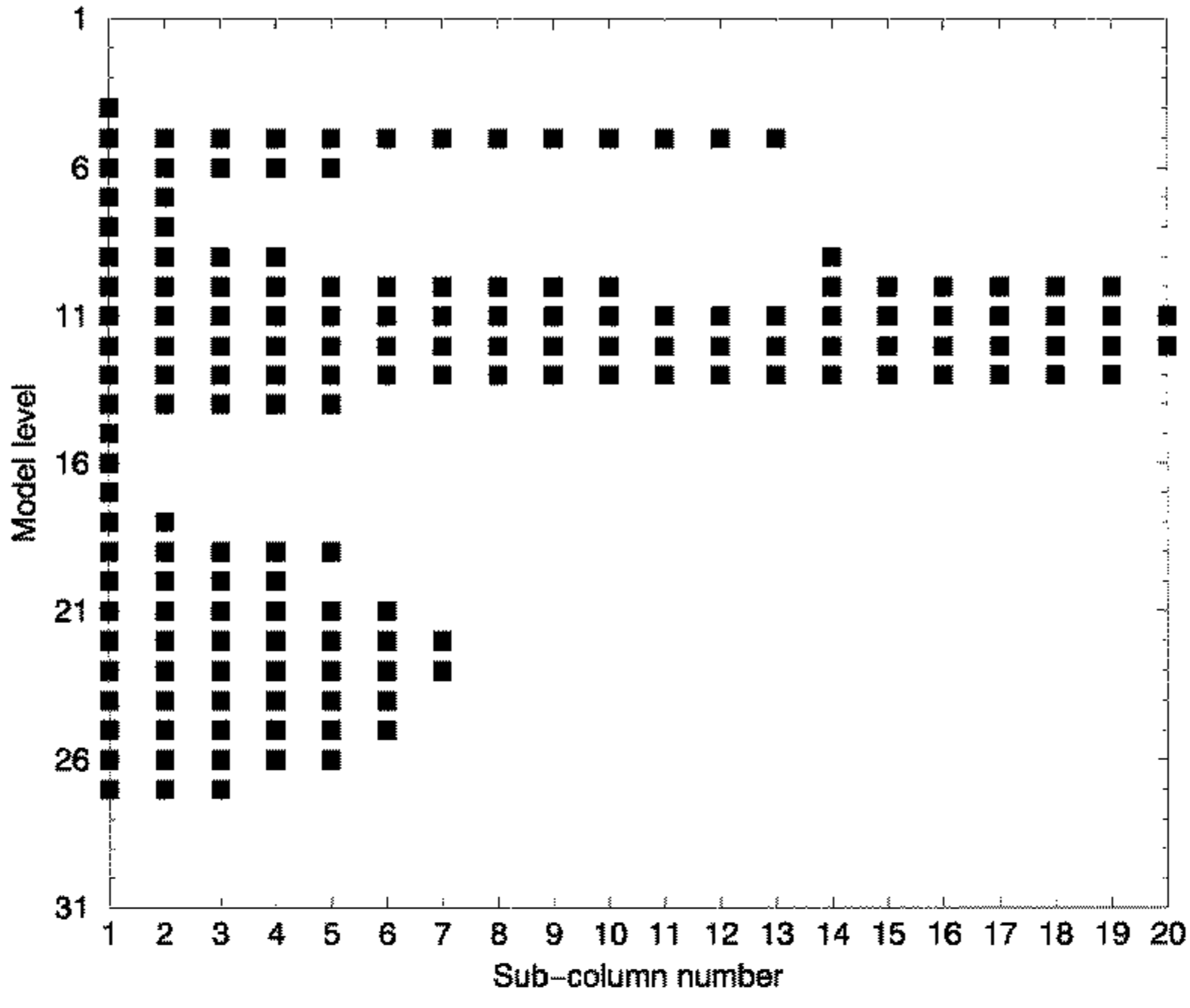

Figure 4. Arrangement, following the subgrid-scale algorithm (see text), of cloudy (black squares) and clear-sky columns for the cloud-fraction profile shown in Fig. 3.

with cloud fraction monotonically increasing or decreasing with height. This is broadly consistent with the data on cloud overlap of Tian and Curry (1989). At each level, the number of sub-columns that contain cloud is defined to be the nearest integer value of $20a^k$.

The use of Eq. (3) provides a total cloud cover, C^k, by applying it from the model top to level k, given the distribution of clouds layer by layer. However, the knowledge of C^k and a^k alone is not sufficient to assign the distribution of cloudy sub-columns unambiguously. In Fig. 4, for instance, it is obvious that C^k does not change below model level 11, where it reaches a value of 1. Hence, the five cloudy sub-columns in level 14, where $a^{14} \approx 0.25$, could be placed in any sub-box without violating (3). Therefore, two additional assumptions are made: (i) in the spirit of maximum overlap for clouds in adjacent levels, clouds are assigned to those sub-columns that contain cloud in the layer immediately above in preference to those sub-columns that do not contain cloud in the layer immediately above but do have clouds higher in the same sub-column, and (ii) the assignment of cloudy boxes begins from the sub-column furthest to the 'left' (i.e. as in Fig. 4) that fulfills (i). Since (ii), especially, is rather arbitrary, sensitivity tests to the placement of cloudy sub-columns were carried out. The 'left' assumption is used as the default assumption for the rest of this study because this is the cloud placement that is implicitly assumed in the E93 scheme.

The amount of liquid and ice at each level is calculated over the mean cloudy area of the grid box in the manner described by Tiedtke (1993). It must then be divided among the cloudy sub-columns of each level. For want of a better method, each cloudy sub-column is assigned the same amount of liquid and ice, assuming a constant in-cloud liquid-water and ice content defined as

$$l^k_{\mathrm{c,int}} = \frac{l^k}{a^k_{\mathrm{int}}}, \tag{4}$$

where l^k is the grid-mean liquid-water and ice content and $a^k_{\rm int}$ is a rounded cloud fraction calculated as the fraction of sub-boxes at each level that contain cloud (it is necessary to use a rounded cloud fraction in the definition of $l^k_{\rm c,int}$ in order to conserve water). After the allocation of the condensed water in the sub-columns, the same microphysical formulae used for the original model are applied to each sub-column separately. That is, for each sub-box the generation and evaporation of precipitation is calculated at each level. Averaging over sub-columns yields grid-mean quantities (precipitation and evaporation rates) that can be compared with the E93 parametrization. In all calculations a homogeneous distribution of temperature at the beginning of the microphysical calculations is assumed, i.e. each sub-column has the same temperature initially. Through melting and evaporation of precipitation the temperature will change differently in each sub-column. The new grid-mean temperature is calculated from the grid-mean melting and evaporation rates that are calculated by averaging over their values in the individual sub-columns.

Two changes are necessary in applying the microphysical formulae to the sub-columns. The first is related to the melting of snow. In the E93 scheme, the amount of melting is limited such that the whole grid box is cooled back to the freezing temperature over a time-scale $\tau = 5$ h, even if precipitation covers only a small fraction of the grid box. For the subgrid-scale precipitation model, the amount of melting is limited such that only the sub-column in which melting occurs can be cooled to the freezing temperature. This implies that, if the fraction of the grid box covered by precipitation is less than unity, the energy available for melting will be smaller in the subgrid-scale precipitation parametrization than in E93. The main effect of this difference is to spread melting further in the vertical.

The second change concerns the evaporation of precipitation. The formula for evaporation of precipitation depends in part on the humidity of the air into which the precipitation is evaporating. Instead of using the grid-mean humidity in the formula (as is done in the E93 parametrization), an estimate of the humidity of the clear portion of the grid box is calculated using the cloud fraction and the grid-mean humidity. Assuming that the temperature inside the cloud is the same as the grid-mean temperature, the grid-mean specific humidity ($q_{\rm v}$) is the sum of the saturation value at the grid-mean temperature in the cloudy portion of the grid ($q_{\rm s}$) and a mean clear-sky value of humidity ($q^{\rm clr}_{\rm v}$):

$$q_{\rm v} = aq_{\rm s} + (1-a)q^{\rm clr}_{\rm v} \ . \tag{5}$$

In the calculation of the evaporation of precipitation in the subgrid precipitation model it is assumed that each cloud-free sub-column has a value of specific humidity equal to the value of $q^{\rm clr}_{\rm v}$ which satisfies (5).

In implementing the subgrid-scale precipitation model, special treatment was given to those grid boxes which have a cloud fraction less than half the size of a sub-column (i.e. $a^k < 0.025$ for a model with 20 sub-columns). Normally, the rounding of cloud fraction to the nearest sub-column would assign all sub-columns as clear sky, and no precipitation could be generated from clouds with these small cloud fractions. In order to avoid problems of that nature, it is required that if the cloud fraction is greater than 0 then at least one sub-box in layer k must be filled with cloud. Water conservation in this case is ensured by redistributing the water quantities over the whole sub-box.

It is worthwhile pointing out that the distribution of the cloudy columns in Fig. 4 should not be interpreted as a spatially contiguous distribution. Shifting all columns randomly, treating each one as a whole in the vertical, will by construction not change the results of the simulation since each column is treated as an independent quantity. It is therefore better to think of the distribution of the cloudy columns as a probability state given the set of rules outlined above.

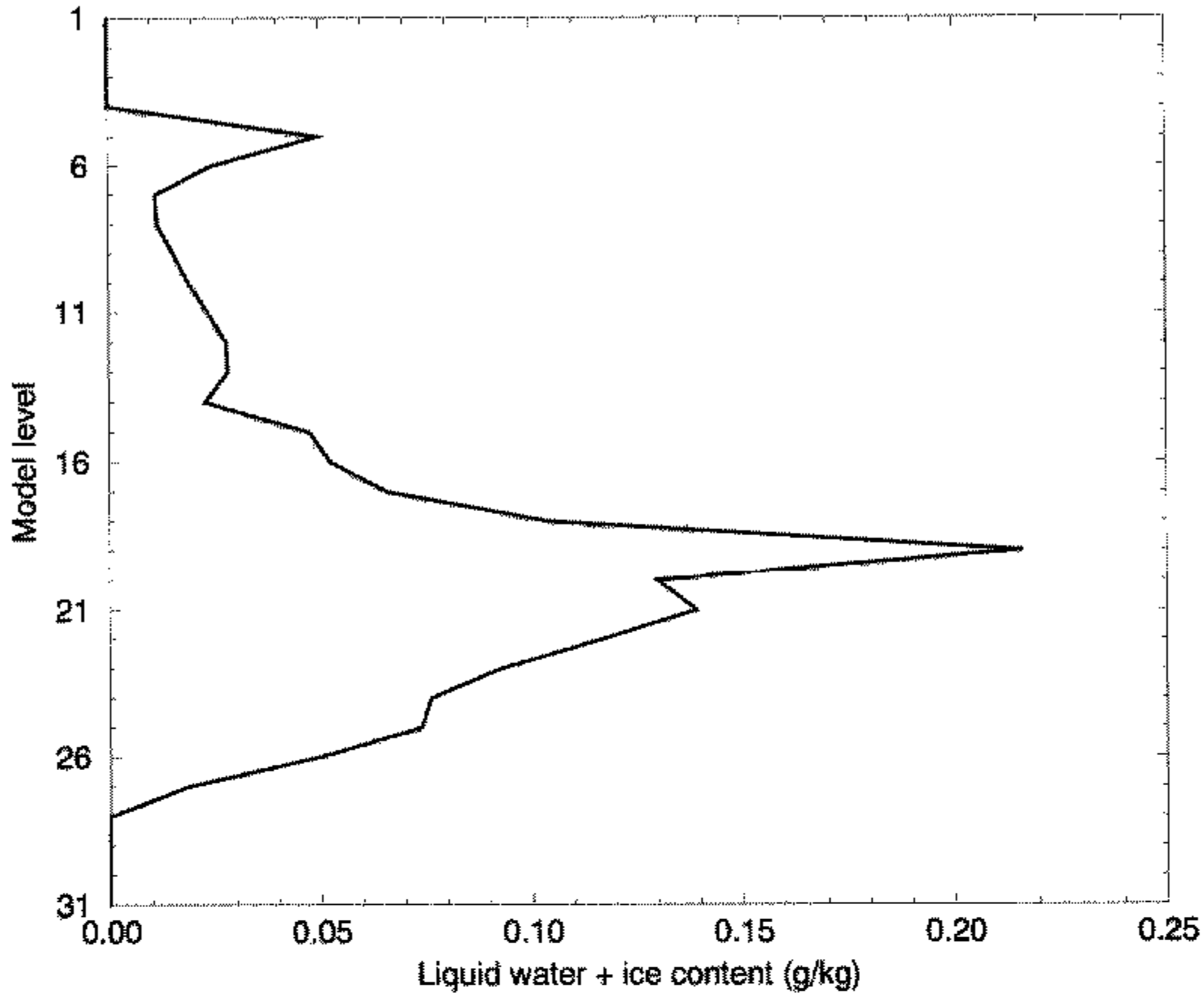

Figure 5. As Fig. 3, but for the grid-mean profile of cloud liquid-water plus ice.

4. Comparison of the subgrid-scale precipitation model with the original E93 scheme

(a) *Single grid-point simulations*

Both the subgrid-scale precipitation model and the E93 parametrization have been used to simulate the precipitation processes at a single grid point. To assess the direct effects of the subgrid model on precipitation related processes, only the first time step of the integration was considered, with all other physical processes switched off. Hence, the simulation was entirely governed by the initial profiles of cloud cover, cloud liquid-water and ice, humidity and the thermodynamic variables. The profiles used are those of the tropical case in Fig. 3. The initial profile of grid-mean cloud water and ice is shown in Fig. 5. The time step used was 15 min, a typical value used in ECMWF's T213L31 model.

The aim of the study is to assess the impact of variations in cloud fraction on cloud microphysics. For this purpose the subgrid model can be regarded as a higher resolution model, which yields more accurate values of precipitation. The E93 parametrization should approximate the subgrid model results if it were to properly account for the subgrid-scale variability of cloud and precipitation. Many factors, including a poor microphysical formulation itself, may cause the results of the subgrid model to be far from reality, but only the differences between the two simulations are of interest for the sensitivity study which is the purpose of this work.

Using the distribution of cloudy and clear-sky sub-columns shown in Fig. 4 the microphysical part of the cloud scheme was integrated separately for each of the sub-columns. A large variation was found in the precipitation fluxes between the different sub-columns. For example, Fig. 6 shows the vertical distribution of precipitation for sub-columns 1 and 6. Sub-column 1, by construction, contains the maximum number of cloudy levels. Hence, precipitation falls through clouds from model level 5 down to model level 27, leading to

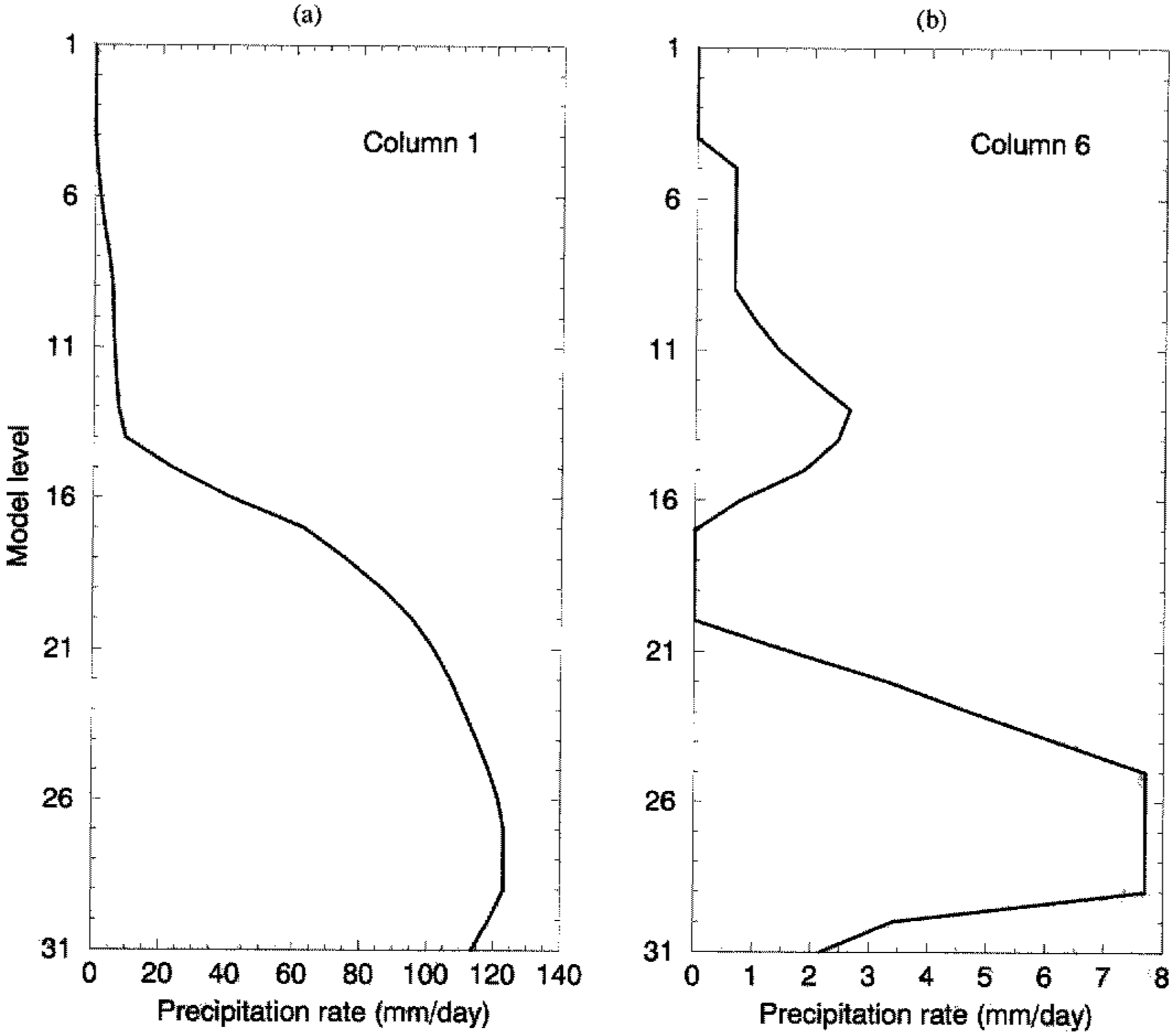

Figure 6. Vertical distribution of precipitation after a single time step of the subgrid precipitation model (a) in sub-column 1 and (b) in sub-column 6. The values refer to precipitation leaving the base of the cloud layer at a given model level.

large amounts of accretion and no evaporation above cloud base. As a consequence, the precipitation rate reaches a maximum of more than 120 mm d^{-1} just above cloud base. In contrast, sub-column 6 contains three cloud layers, extending over one, four and five model levels respectively, separated by layers of clear sky. Precipitation forms first in model level 5. Although levels 6 through 9 contain unsaturated air, the precipitation rate remains constant until the next cloudy layer (model level 10). No sublimation occurs between levels 6 and 9 because the E93 scheme assumes that precipitation cannot evaporate when the relative humidity exceeds a critical value of 80%. After leaving the base of the second cloud layer, evaporation of precipitation results in the total depletion of the precipitation at level 17 so that no precipitation reaches the lowest cloud layer with its top at level 21. This is an example of the importance of the seeder–feeder mechanism; no precipitation reaches the low cloud from above so that only the warm-phase microphysics is important for the development of the lowest cloud layer. The precipitation reaching the surface in this sub-column (slightly more than 2 mm d^{-1}) is entirely due to conversion processes in the lowest cloud layer, and has been reduced by evaporation in the sub-cloud layer.

By counting the sub-columns that contain precipitation at each level it is possible to derive the fraction of the grid box covered by precipitation (from now on this is referred to as the precipitation fraction, a_P). This parameter is used in several ways in existing parametrization schemes (Bechthold *et al.* 1993; Tiedtke 1993; Rotstayn 1997). For example, the evaporation of precipitation in model level k in the E93 parametrization is described as:

$$E_P^k = \max(a_P^k - a^k, 0) \times 5.44 \times 10^{-4}(q_s^k - q^k) \left\{ \left(\frac{p^k}{p_{\text{surf}}} \right) \frac{1}{5.9 \times 10^{-3}} \frac{P^k}{a_P^k} \right\}^{0.577}, \quad (6)$$

where p_{surf} is the surface pressure. The precipitation fraction, a_P^k, appears twice in Eq. (6). Firstly, it is used to calculate the area over which evaporation can occur, $a_P^k - a^k$, assuming maximum overlap between precipitation and cloud. Secondly it determines the local precipitation rate in the area that contains precipitation as P^k/a_P^k, where P^k is the grid-mean precipitation rate. The E93 parametrization contains a description of a_P^k which can be expressed as

$$a_P^k = \max \left\{ a_P^{k-1}, \left(\frac{a^k \Delta P + a_P^{k-1} P^{k-1}}{\Delta P + P^{k-1}} \right) \right\}, \quad (7)$$

where a_P^{k-1} is the area covered by precipitation leaving the level above and is thus the area covered by precipitation entering level k, P^{k-1} is the amount of precipitation leaving level $k-1$, ΔP is the amount of precipitation generated in level k, and a^k is the cloud fraction at level k. Evaporation of precipitation does not alter a_P, except when precipitation evaporates completely.

Figure 7 compares the precipitation fraction diagnosed from the subgrid model with that given by (7). The parametrization following (7) does not correctly capture the vertical distribution of a_P. There are two major differences; in the anvil region (model level 11 to 16), the precipitation fraction is underestimated by (7), and below those levels it is considerably overestimated. The reasons for these differences lie in the construction of (7). In this parametrization, a_P^k is determined as a weighted average of the precipitation fraction of level $k-1$ and the cloud fraction in level k, where the weights are the precipitation flux in layer $k-1$ and the change in precipitation flux due to microphysical processes in layer k. This weighting was introduced to prevent levels that do not contribute to precipitation from being contributors to a_P. In the example shown, this parametrization underestimates a_P in the anvil part since the precipitation added to the flux in that part (ΔP) is not large enough compared to the incoming flux from above (P) to increase the precipitation fraction to the correct value of 1. However, as is shown below, a more important difference is the overestimation of a_P below level 16. This results from the maximum statement in (7), which prevents a reduction in a_P unless all the precipitation evaporates. This has an impact on the evaporation of precipitation because the area over which precipitation is allowed to evaporate is defined as $a_P^k - a^k$.

Figure 8 compares the grid-mean evaporation rates of the subgrid and E93 models. The grid-mean values for the subgrid model are calculated by averaging over the values of the individual sub-columns. As expected, large differences exist in the middle troposphere with a strong overestimation of evaporation by the E93 scheme. The most likely explanation of this difference is that an overestimation of a_P also leads to an overestimate of the amount of precipitation available for evaporation. To test whether this is the major source of the difference, the simulation of the E93 scheme was repeated with the precipitation fraction prescribed to be that diagnosed from the subgrid precipitation model (see Fig. 8). At least in this case, the overestimation of a_P did cause most of the large differences in evaporation

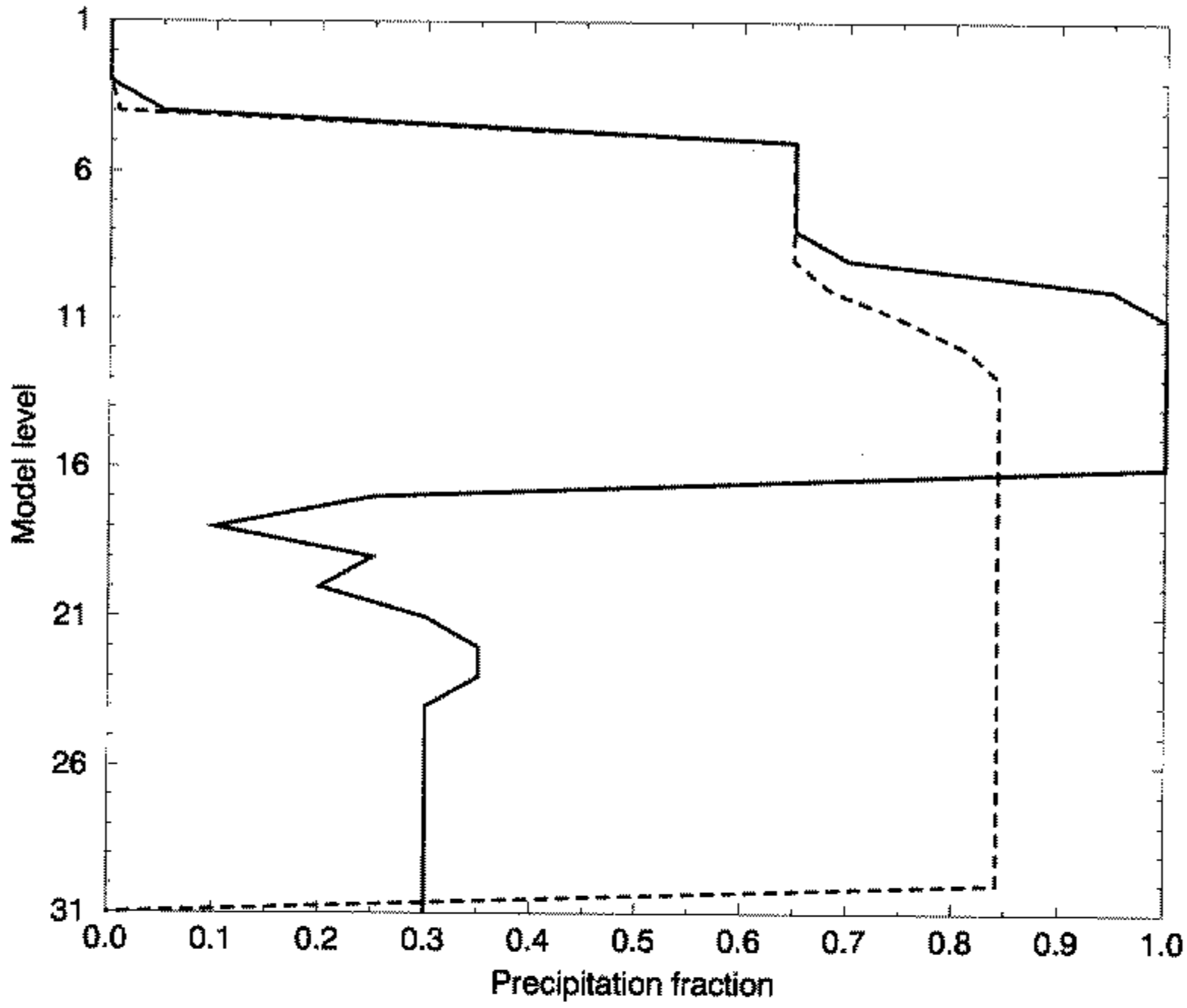

Figure 7. Precipitation fraction as simulated by a single time step of the subgrid precipitation model (full line) and the E93 scheme (dashed line). The values refer to the fraction covered by precipitation at the bottom of the cloud layer at a given model level.

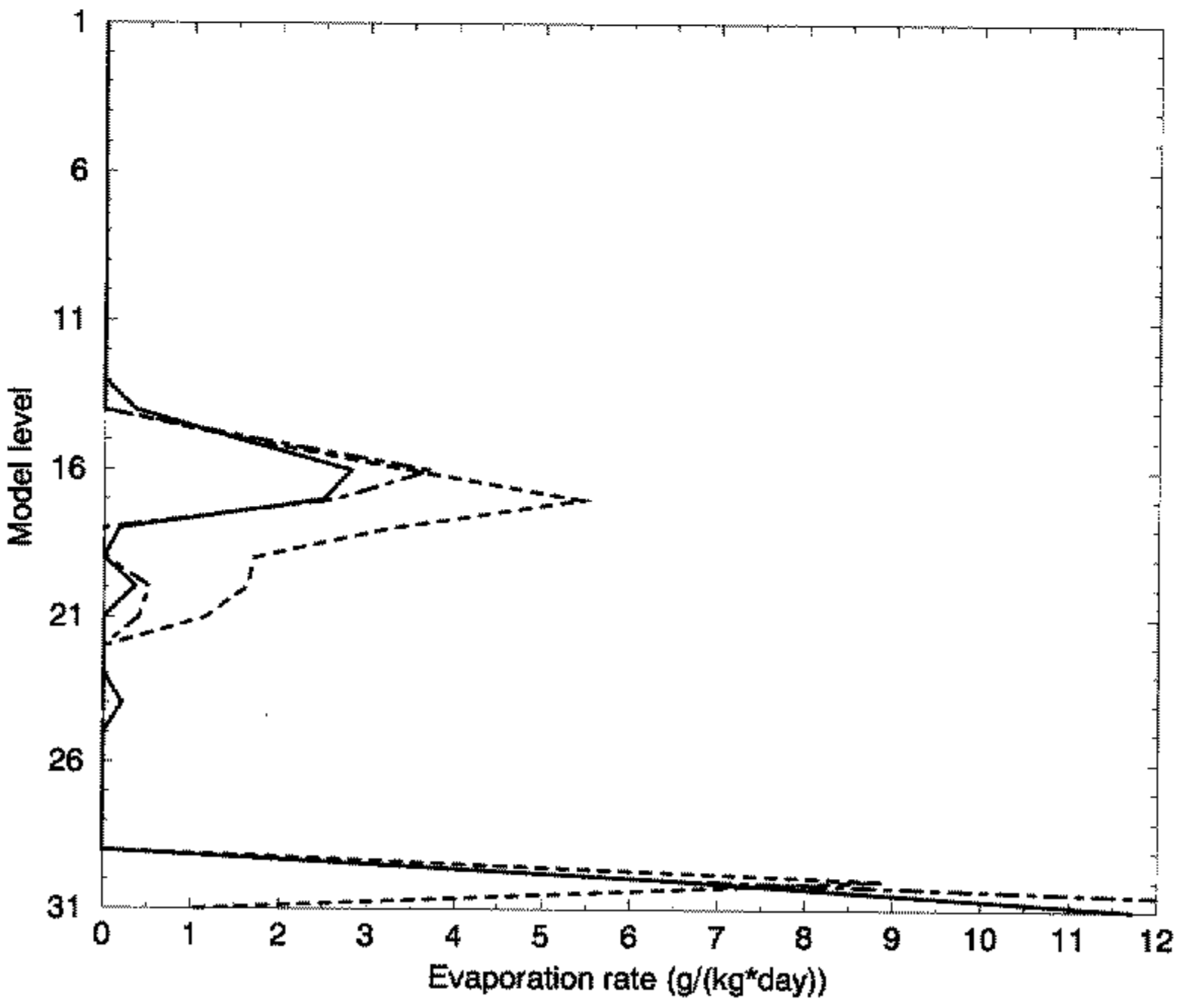

Figure 8. Evaporation rate as simulated by a single time step of the subgrid precipitation model (full line), the E93 scheme (dashed line), and the E93 scheme with a prescribed precipitation-fraction profile (dot-dashed line) (see text).

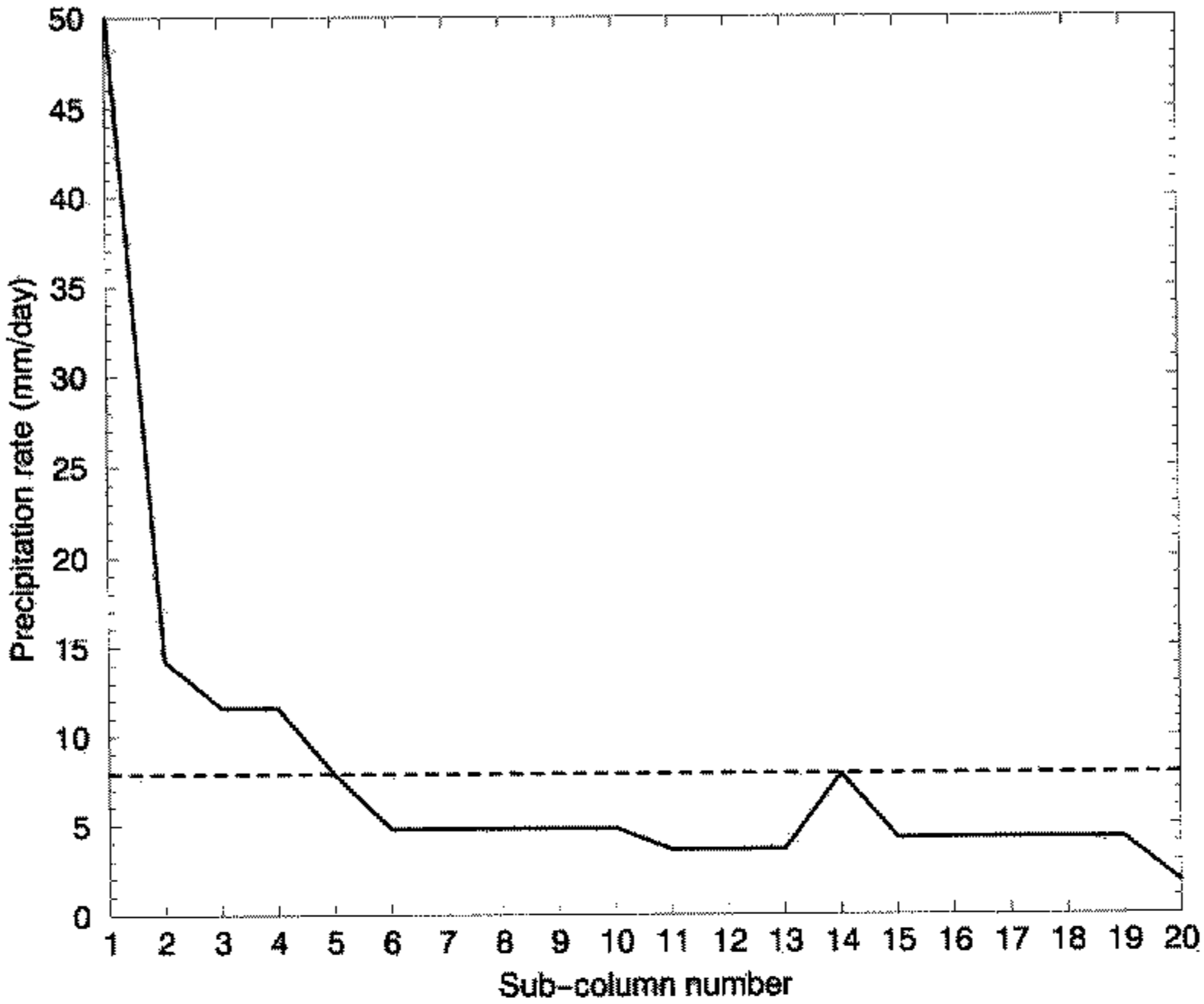

Figure 9. Precipitation rate at the top of the cloud layer at model level 16, as simulated by a single time step of the subgrid model (full line) and the E93 scheme with a prescribed precipitation-fraction profile (dashed line) (see text).

of precipitation in the middle troposphere. However, there are still major differences, such as at model level 16.

It is worthwhile investigating the cause for this difference, since model level 16 is the only level where the 'true' a_P is much larger than the cloud fraction, so that a significant area of the grid box is subject to evaporation of precipitation. Because the formula for evaporation depends on the local precipitation rate in the volume undergoing evaporation of precipitation, an overestimation of evaporation could result from an overestimation of the precipitation rate in this volume. Figure 9 shows the distribution of the precipitation rate in model level 16 for the subgrid model and the E93 scheme with prescribed a_P, just before the parametrization of evaporation is calculated. Since $a^{16} \approx 0.07$, only the first sub-column is assumed to be cloudy while $a_p^{16} = 1$. It is evident that for most of the sub-columns undergoing evaporation (columns 2 to 20) the precipitation rate before evaporation is lower than the mean precipitation rate given by the E93 scheme with prescribed a_P. In fact, excluding the sub-column with the largest precipitation rate (column 1), which is not subject to evaporation since it is cloudy, the average precipitation rate of the subgrid model is 5.8 mm d^{-1} as compared with 7.9 mm d^{-1} for the E93 model. This difference directly contributes to the difference in evaporation rate at level 16. This suggests that a very important error source in the E93 parametrization, even with a perfect simulation of a_p^k, may be that the local precipitation rate in the region undergoing evaporation is significantly less than the grid-mean precipitation flux divided by the precipitation fraction. Using only a grid-averaged precipitation flux implies the averaging of the fluxes inside the cloud (where it increases downwards due to conversion and accretion) and outside the cloud (where it decreases downwards due to evaporation). This averaging leads to an artificial horizontal transport of precipitation from generally larger values inside cloud to generally smaller

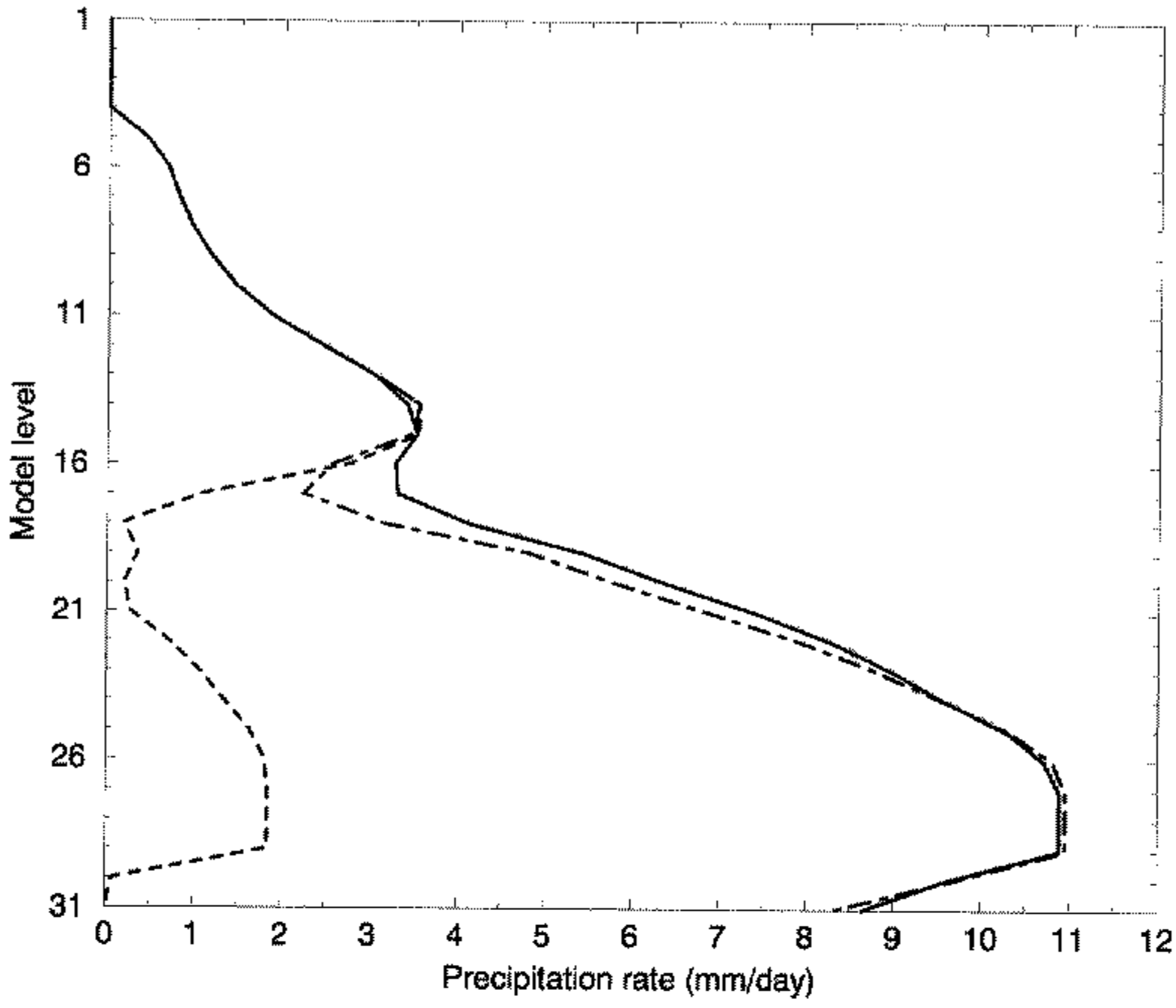

Figure 10. As Fig. 8, but for the precipitation rate.

values outside cloud, and thereby to an overestimation of evaporation. This problem will tend to occur at all cloudy levels having both precipitation and $a_p^k > a^k$.

Figure 10 compares the grid-mean precipitation flux for the same simulations as in Fig. 8. Large differences between the subgrid and the E93 model begin at level 16 and increase downwards. The precipitation reaching the surface differs by more than 8 mm d^{-1} (leading to consequential differences in the net latent heating of the column), with no precipitation at all reaching the surface in the E93 scheme. Forcing the precipitation fraction to be that diagnosed from the subgrid model alleviates most of the discrepancies, except near level 16.

(*b*) *Global model*

Several errors in the parametrization of microphysical processes that result from improperly accounting for the subgrid-scale distribution of cloud and precipitation have been identified for a single case. To assess the generality of these results, the global ECMWF model was integrated for one time step ($\Delta t = 60$ min) at spectral resolution T63. The reason for using only one time step was again to establish the direct effect of the subgrid model on the model physics without allowing feed-backs to occur. The precipitation fraction, evaporation rate, and precipitation rate were compared using the subgrid precipitation model and the E93 parametrization for the initial conditions of the ECMWF operational model on 12 UTC 1 July 1997. The initial distribution of cloud fraction for this time is shown in Fig. 2.

Figure 11 compares the zonal means of the precipitation fraction analysed from the simulations with the subgrid model and the E93 scheme. The differences between the two models are large, with the most significant differences occurring in the tropics. As with the single-column case, the E93 scheme underestimates the high-level a_P, but largely

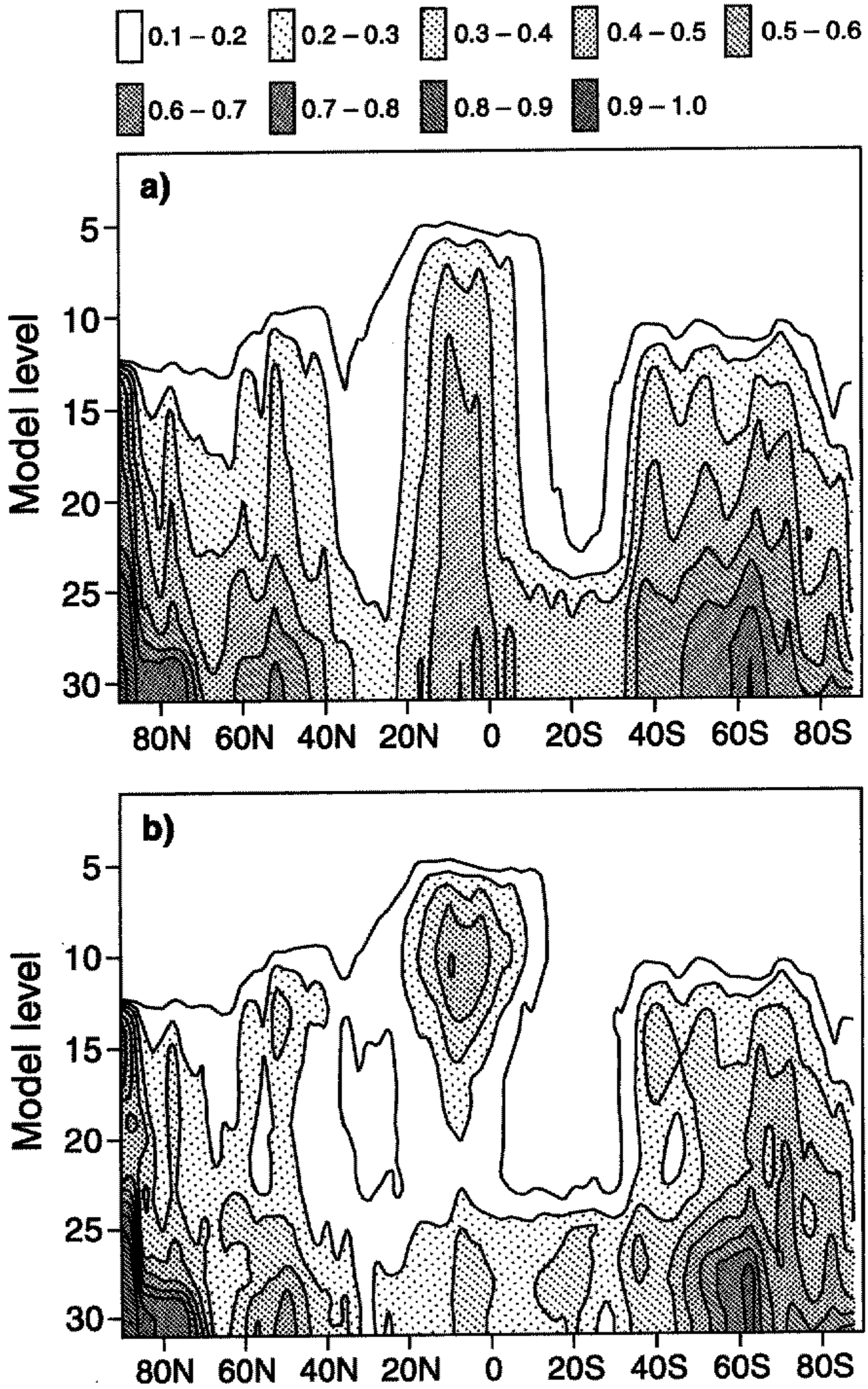

Figure 11. Zonal-mean distribution of the precipitation fraction for the first time step of an integration with the global T63L31 model for 12 UTC 1 July 1997 shown as a function of latitude and model level using (a) the E93 scheme and (b) the subgrid model.

TABLE 1. GLOBAL MEANS OF COMPONENTS OF THE HYDROLOGICAL CYCLE (LARGE-SCALE ONLY) FOR THE FIRST TIME STEP OF AN INTEGRATION OF THE GLOBAL T63L31 MODEL WITH THE E93 SCHEME AND THE SUBGRID PRECIPITATION MODEL.

	E93 scheme	Subgrid model
Liquid-water and ice content (mm)	0.126	0.126
Formation of precipitation (mm d^{-1})	2.67	2.65
Evaporation of precipitation (mm d^{-1})	0.99	0.78
Surface precipitation (mm d^{-1})	1.68	1.87

overestimates the mid-level a_p. The differences in the extratropical regions are smaller, although the subgrid model yields a smaller a_p in the middle troposphere. In the extratropics one could speculate that vertically varying cloud fraction plays a smaller role because the cloud fraction tends to be more uniform, e.g. in frontal cloud systems.

With errors in a_p similar to those in the single-column simulation, similar errors in the grid-mean evaporation and precipitation rates can also be expected for the global model. Figure 12 shows the zonal mean of the grid-mean evaporation rate for both the E93 and the subgrid model, and Fig. 13 the zonal-mean surface large-scale precipitation. The strong overestimation of evaporation in the middle troposphere in the tropics is evident and leads to a difference of up to 1.5 mm d^{-1} in zonal-mean large-scale precipitation, equivalent to a latent-heat release of more than 40 W m^2 .

Table 1 summarizes the global-mean values for some of the components of the hydrological cycle for the first time step. Starting from the same initial liquid-water plus ice content (0.126 mm) both models generate about the same amount of precipitation ($\approx$ 2.65 mm d^{-1}). However, the evaporation rate for the subgrid model is about 20% smaller than that of the E93 model leading to about 0.2 mm d^{-1} more large-scale precipitation. The difference in the net latent-heat release due to large-scale precipitation constitutes an extra forcing for the model, and it could certainly affect a full global model simulation. As this study concentrates on the direct physical effects of vertically varying cloud fraction, a discussion of the effects on a full simulation of the model climate is beyond its scope and will be carried out elsewhere.

(c) *Sensitivities*

Before ascribing differences between the E93 scheme and the subgrid model to errors in the parametrization, it is necessary to establish that the results of the subgrid model are not sensitive to arbitrary assumptions in the construction of the model. The two main assumptions that might influence the results are the placement of cloudy boxes and the number of subgrid columns used.

As already mentioned in section 3, the horizontal distribution of the columns in Fig. 4 should not be interpreted as a spatial distribution. In fact if all the columns were redistributed randomly the result of the precipitation calculations would not change at all. It is, therefore, more appropriate to consider the distribution of the columns as a probability distribution rather than as a spatial one. One of the constraints for the distribution is the cloud-overlap assumption for the grid box. This determines how many of the cloudy subboxes in a model level need to be placed in columns containing clouds in at least one of the higher levels in the column, and how many in columns that contain clear sky in all higher levels of the column. However, as explained above, the exact placement within each of these two groups (referred to as 'cloud under cloud' and 'cloud under clear sky') is ambiguous. The distribution used so far in the study (Fig. 4) was built by assigning higher probabilities

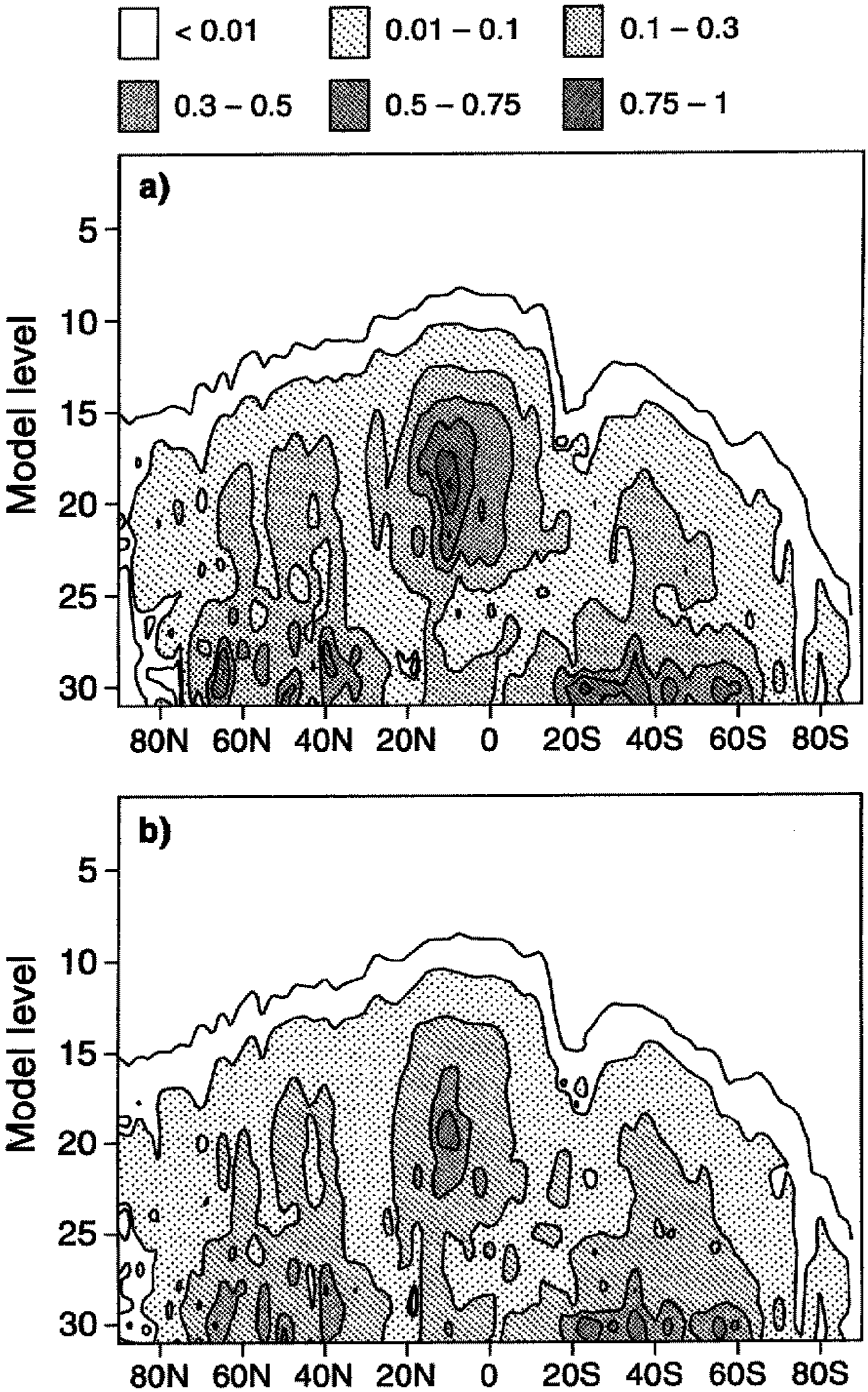

Figure 12. As Fig. 11, but for the zonal mean of the grid-mean evaporation rate (g $kg^{-1}d^{-1}$).

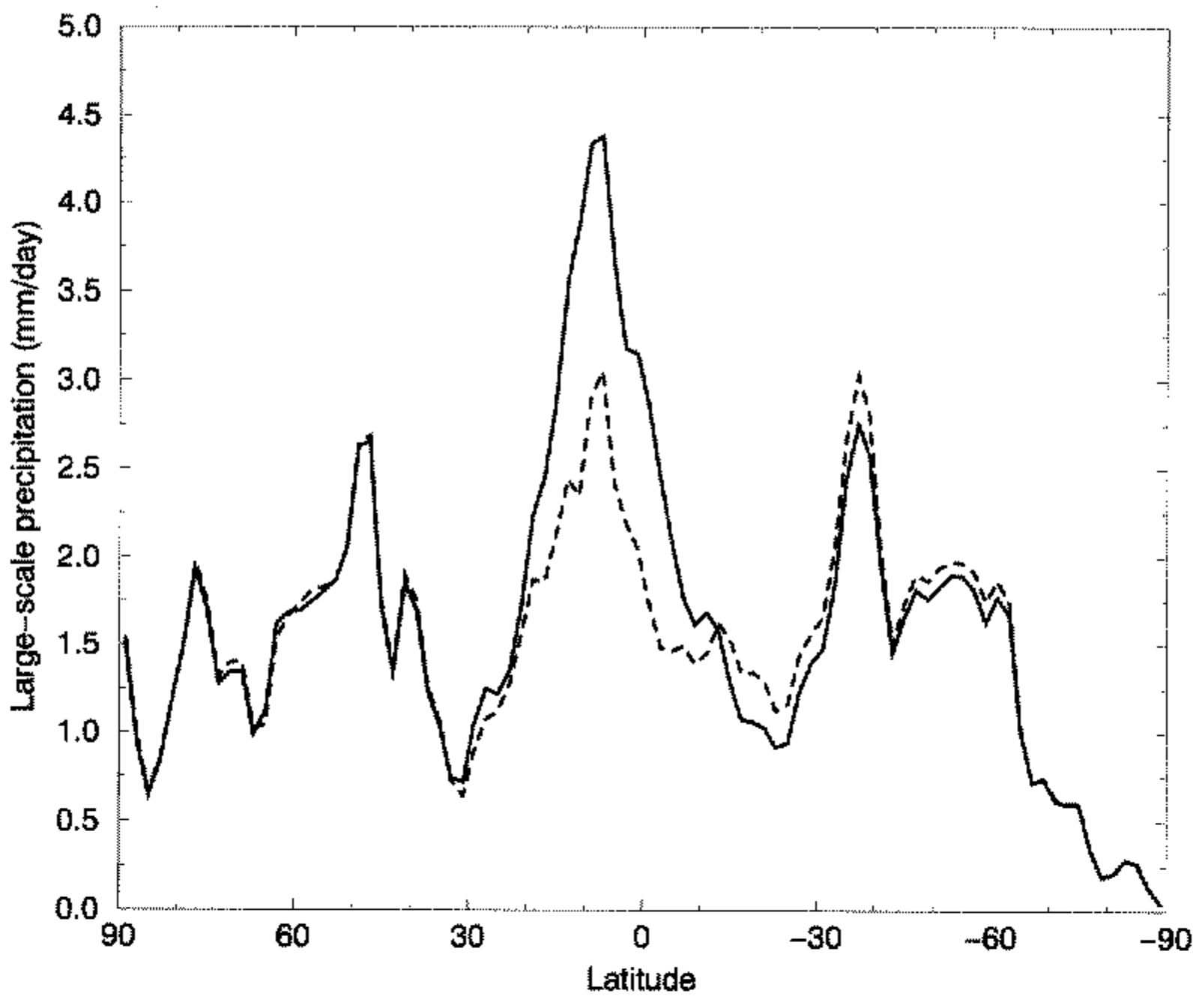

Figure 13. Latitudinal variation of the zonal-mean large-scale precipitation rate at the surface for the first time step of an integration of the global T63L31 model using the subgrid precipitation model (full line) and the E93 scheme (dashed line).

to certain columns being cloudy. For instance, in the case of cloud under cloud, cloudy boxes were preferentially placed in columns that contain cloud in the layer immediately above. Furthermore, for each of the two groups, the probability is artificially a function of the column index because boxes are filled preferentially from the left (Fig. 4). In order to study the impact of these assumptions on the grid-mean results, these preferences were removed and new clouds were placed randomly within each group. Note, however that the maximum-random cloud-overlap assumption for the grid box as a whole as expressed in (3) was retained. The precipitation rate for the one-time-step integration in the tropics differs between these two column-placement options (for convenience named left and random) by about 1 mm d^{-1} (Fig. 14). The smaller precipitation rates in the random case result from smaller accretion rates caused by the removal of the 'tower' of cloud that exists in the left-placement case in column 1 (Fig. 4). The differences between the results from the two cloud distributions are, however, much smaller than the differences between the results from the subgrid model and the E93 parametrization (cf. Fig. 10). The global-model results (not shown) confirm the results of the single-column simulation.

Another important sensitivity test is whether the results of the subgrid model depend on the number of sub-columns used. Since the subgrid model rounds the actual model cloud fraction to a multiple of the sub-column size, which is obviously a function of the number of columns used, it is desirable to use as many sub-columns as possible to minimize rounding errors. However, if one expects the model cloud fraction to be accurate to not more than 0.05 than the use of, say, 100 sub-columns would not be sensible. The differences between simulations with different numbers of sub-columns (Fig. 15) are smaller than the differences between simulations with different cloud placements (Fig. 14), and certainly much smaller than the differences between the subgrid model and the E93 scheme (Fig. 10). These results are confirmed by the global-model experiment (not shown).

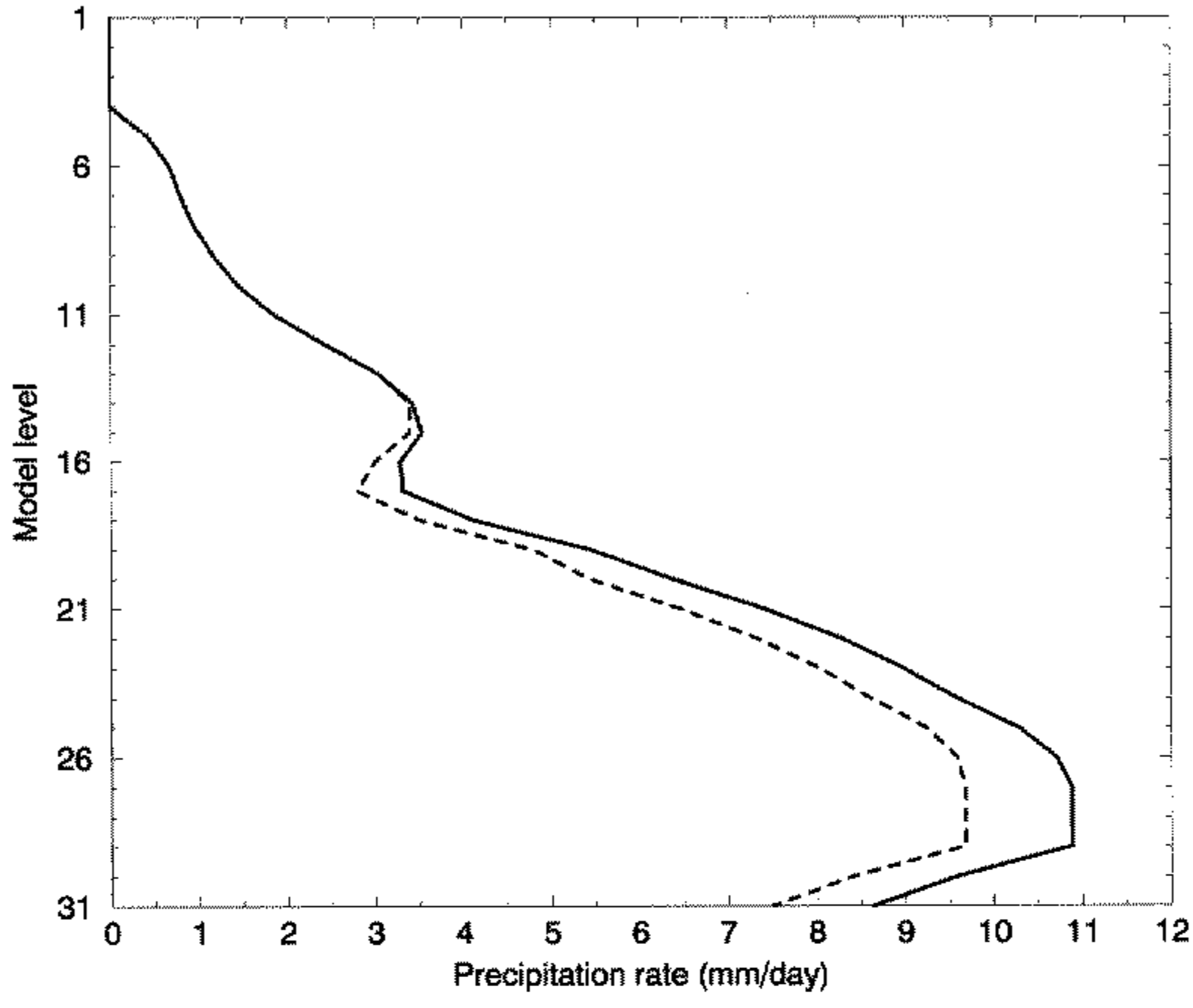

Figure 14. Precipitation rate as simulated by a single time step of the subgrid precipitation model with 'left' (full line) and 'random' (dashed line) cloud placements (see text). Both simulations assume the same maximum-random cloud-overlap assumption.

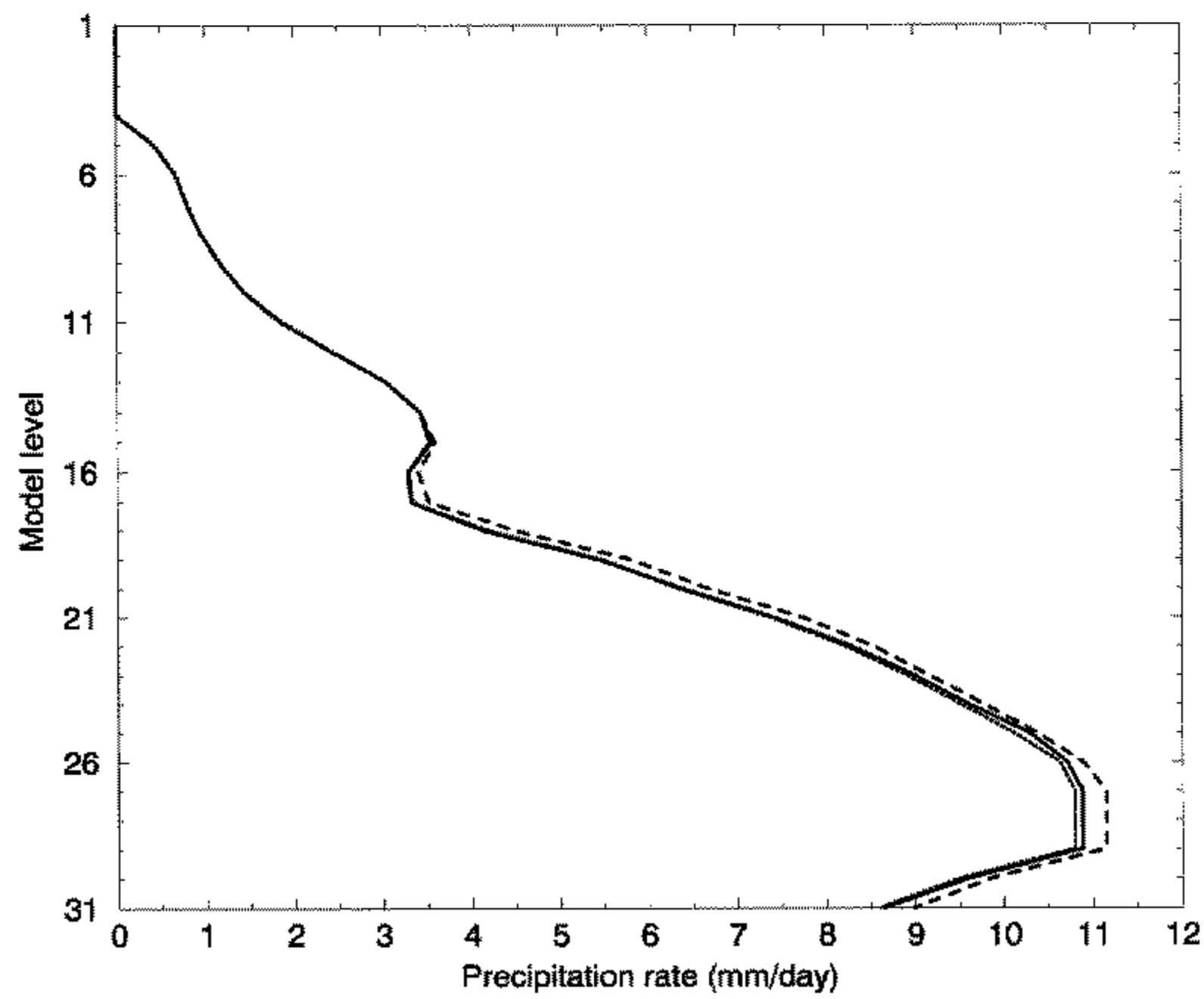

Figure 15. Vertical profile of the precipitation rate as simulated by a single time step of the subgrid precipitation model using 20 (full line), 10 (dashed line) and 100 (dotted line) sub-columns.

The use of different values for specific humidity in the calculations of precipitation evaporation (q_v in the E93 parametrization and q_v^{clr} in the subgrid model) might also contribute to the differences shown. Therefore the single-column calculations were repeated using q_v in the subgrid model and q_v^{clr} in the E93 scheme. The results (not shown) indicated little sensitivity to the choice of specific humidity for the subgrid model, but increased the evaporation rates in the E93 parametrization, leading to even larger discrepancies between the two simulations. The different behaviour of the two schemes can be explained by their very different simulation of precipitation fraction. In the case of the subgrid model, the precipitation fraction decreases rapidly below the anvil so that evaporation of precipitation can occur in only few sub-columns, or not at all. Hence the small sensitivity of this scheme to the choice of specific humidity. In contrast, the E93 parametrization creates large areas of evaporation below the anvil because of its overestimation of precipitation fraction. Hence changing the specific humidity used in the evaporation calculations exerts a larger influence.

All the sensitivity tests described so far used the maximum-random overlap cloud-overlap assumption of the current E93 model. However, altering this assumption would indicate what role the cloud-overlap assumption plays when using a more complex treatment of vertically varying cloud fraction. It should be noted that, since the E93 parametrization uses maximum-random overlap for clouds (and implicitly assumes a maximum overlap of cloud with precipitation), a comparison of the E93 scheme with the results of the subgrid model with a different overlap assumption would not be appropriate. Hence, the main purpose of such a test is to establish the sensitivity of the subgrid scheme (and, hopefully, of the parametrized cloud microphysics as well) to the cloud-overlap assumption. Figure 16 shows the zonal-mean precipitation of three one-time-step integrations of the global model using the subgrid precipitation scheme with maximum-random, maximum and random overlap. All integrations use the default (left) method to place cloudy boxes. It is evident that a large difference exists between the random-overlap and the other two overlap assumptions. The reason for the large reduction in precipitation when using random overlap is the horizontal spreading out of the cloud which leads to higher evaporation and lower accretion rates. The implications of this result are discussed below.

5. Summary and discussion

This study has used a subgrid precipitation model to assess the performance of the 1993 ECMWF stratiform precipitation scheme in the presence of vertically varying cloud fraction. The basic idea of the subgrid scheme is to divide the model grid box into several sub-columns and, after distributing the parametrized cloud such that each column represents either cloudy or clear sky, to solve the microphysics part of the parametrization for each column separately. Extensive comparisons between the subgrid model and current E93 parametrization have been carried out in the context of one-time-step experiments for both the single-column model and the global model. One-time-step simulations have been preferred to longer model integrations because they help the understanding of the direct implications of the different treatment of cloudiness variations in the vertical.

The comparison has revealed two important shortcomings of the E93 parametrization:

- there is an erroneous simulation of precipitation fraction;
- large truncation errors are introduced by averaging the precipitation flux over the whole precipitation area. This average results from the assumption that the local precipitation rate equals the grid-mean precipitation rate divided by the precipitation fraction.

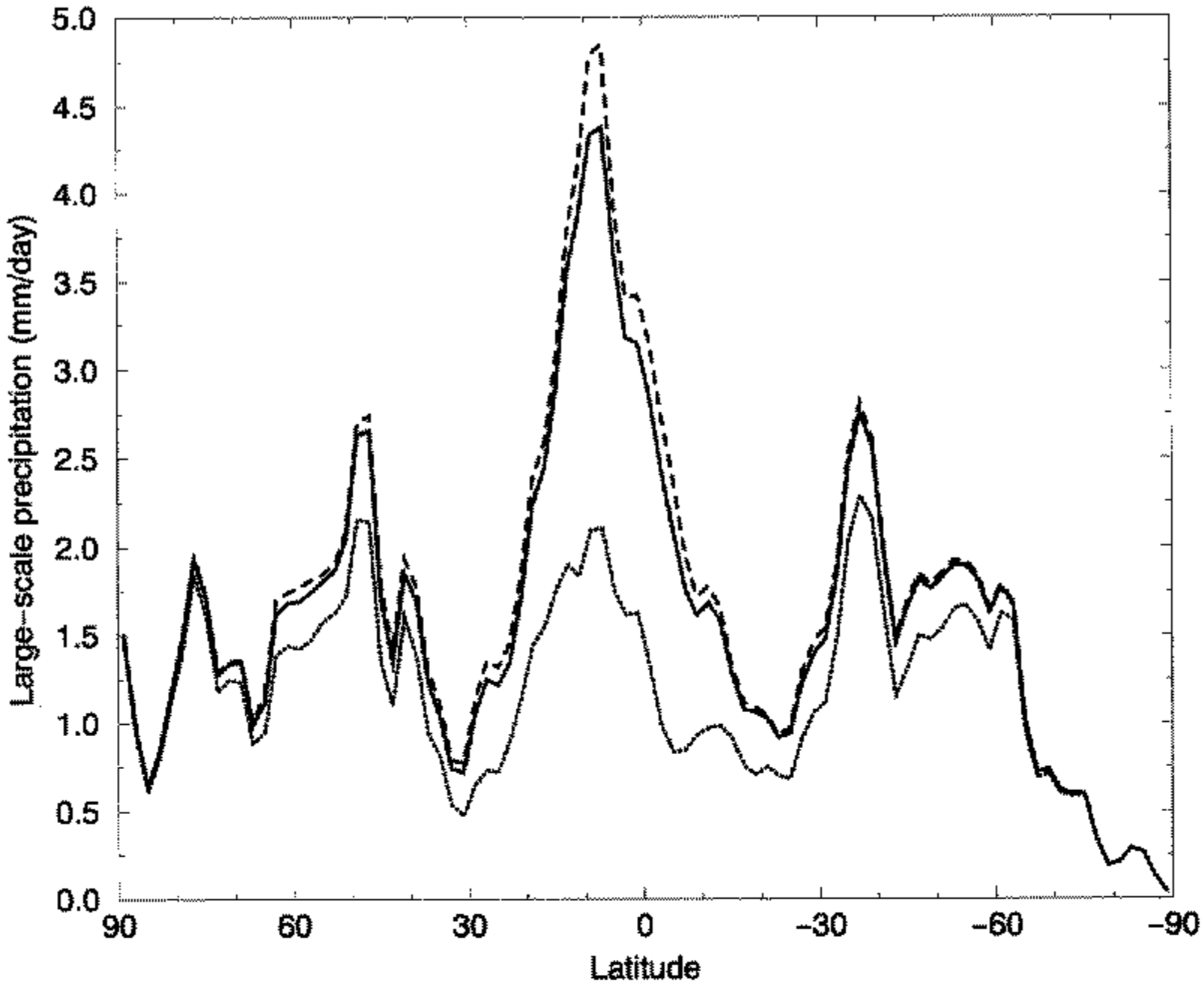

Figure 16. Zonal-mean large-scale precipitation rate for the first time step of an integration of the global T63L31 model using the subgrid precipitation model with maximum-random (full line), maximum (dashed line), and random (dotted line) cloud-overlap assumptions.

The main effect of these errors has been found to be an overestimation of evaporation (an important finding because GCMs are known to be very sensitive to the parametrization of evaporation). A generalization of these results to other parametrization schemes is difficult, since little has been revealed in the literature about the details of the treatment of cloud and precipitation overlap when parametrizing stratiform precipitation in connection with cloud fraction. An exception is the study of Rotstayn (1997), which addresses the first item on the list above. However, to the authors knowledge, no parametrization has so far attempted to address the second item above; this can be equally important once a good parametrization of the precipitation fraction has been found.

Several sensitivity studies were carried out to estimate the influence of assumptions used in the construction of the subgrid model. Little sensitivity has been found to the number of sub-columns used, as long as the number is large enough to avoid large rounding errors; a number greater than ten appears sufficient in the ECMWF model. There was a slightly larger sensitivity to the way the sub-columns were filled with cloud once the general cloud-overlap assumption had been enforced. Although larger than the sensitivity to the number of sub-columns, these differences were small compared with the differences between the subgrid model and the E93 parametrization, thereby giving some confidence in the findings of the comparison.

A large sensitivity to the general overlap assumption has, however, been found. A change from maximum-random to random overlap led to a dramatic decrease of the stratiform precipitation rate over the whole globe. This is not surprising since the random-overlap assumption maximizes the spreading out of the clouds in the grid box, thereby reducing the accretion rate and increasing the evaporation rate. It is necessary to stress

again that this large sensitivity does not invalidate the general results of the study, since the E93 parametrization uses a maximum-random overlap of clouds and, therefore, cannot be sensibly compared with a subgrid scheme that uses a different cloud-overlap scheme. However, the large sensitivity stresses the need for improved knowledge on the best way of overlapping clouds when introducing a treatment of vertically varying cloud fraction into both the radiation and the microphysics parametrizations. It is also noteworthy that, given the relatively high vertical resolution of the ECMWF model (around 40 hPa in the free troposphere), the random-overlap assumption does not seem appropriate.

In the light of the current tendency to improve microphysical parametrizations in large-scale models by introducing more and more complex bulk microphysical schemes, the results here suggest that great care has to be taken when addressing the fact that modern cloud parametrizations can produce large variations in cloud fraction in the vertical. A balance between the sophistication of the cloud microphysics and the sophistication of the cloud macrophysics (such as the cloud and precipitation fractions and their overlaps) would seem to be prudent.

A necessary step is, of course, the validation of the vertical cloud variation produced by the parametrization. Little is known about the performance of cloud schemes for GCMs in that respect, although a recent first study by Mace *et al.* (1998), which compares model clouds to radar observations at the model's vertical resolution on an hourly time-scale, shows encouraging results for the ECMWF model. The study is, however, limited to cloud-occurrence statistics at one location and during one season and, therefore, does not cover the variety of cloud situations encountered globally. Wang and Rossow (1995) have presented some general statistics on cloud layering based on radiosonde observations at 30 sites. A qualitative comparison of the ECMWF model results with their findings can be found in the appendix. It confirms the ability of the model to produce reasonable vertical cloud structures.

Observations of precipitation fractions near the surface have recently been derived from radar measurments by Sui *et al.* (1997) during the Tropical Ocean and Global Atmosphere project's Coupled Ocean–Atmosphere Response Experiment*, and these could prove extremly useful in the validation of this crucial parameter. Further guidance is also to be expected through the intercomparisons of single-column versions of GCMs with cloud-resolving models as they are currently performed within the GEWEX (Global Energy and Water-cycle Experiment) Cloud System Study* and the Atmospheric Radiation Measurement programme*.

There is a variety of possible applications of the subgrid model developed for this study. The most obvious is its direct implementation within a GCM, although this might not be practical because of the extra calculations introduced by the multiple integrations of the microphysics parametrization. Including the subgrid model with 20 sub-columns in the ECMWF T63L31 model increased the computer time by about 10% in a 4-month integration. One can speculate that this increase would be even larger if more sophisticated microphysical parametrizations were used. Nevertheless, the subgrid model can provide guidance in the development of the parametrization of the effects discussed. The results above indicate that such a parametrization has to contain at least two components: a treatment of precipitation fraction and a technique that avoids the averaging of the precipitation flux over the whole precipitation area, for instance by introducing separate clear-sky and cloudy precipitation fluxes. A parametrization using the results of this study has been developed at ECMWF; it will be described in a future paper which will also address the impact of the changes in precipitation parametrization on the model climate.

* A component of the Global Climate Research Programme

Other applications of the subgrid model include the testing of the radiation parametrization in terms of its treatment of vertically varying cloud fraction, given a fixed overlap assumption (Liang and Wang 1997). Developing suitable methods of treating cloud inhomogeneity, using the subgrid model for guidance, also appears to be a potential application (e.g. Tiedtke 1996). There is no doubt that, with the improvements in cloud parametrization over the last decade, more thought has to be given to the role of variations of cloud within single-column and subgrid models of the types presented here, and to how these can be used in the development of appropriate parametrizations of their effects.

Acknowledgements

We are grateful to Drs A. Hollingsworth, M. Miller and A. Beljaars for their comments on early versions of this manuscript. We would also like to thank two anonymous referees whose reviews led to further improvement of the manuscript.

Appendix

In this appendix, the statistics of cloud vertical structure in the ECMWF model are compared with those inferred from an analysis of radiosondes presented by Wang and Rossow (1995). Histograms of the number of cloudy layers in a column, their thicknesses, and the separation distances between cloud layers in vertical columns containing multi-layered clouds are presented. In comparing model data with observations, it is assumed that if cloud occurs in vertically adjacent model layers then they are part of a single cloud layer. Cloud is said to occur in a model layer when the cloud fraction in that layer is greater than a threshold value, here taken as 10^{-5}. For example, if cloud occurs in model layers 6, 7, 8, and 23, then there are two cloud layers, one with a thickness of 3 model layers and the other with a thickness of 1 model layer, and a separation distance between the layers of 14 model layers.

The histogram in Fig. A.1 is taken from a 24-hour forecast of the current ECMWF model run with 31 vertical levels at T63 horizontal resolution. Approximately a third of the cloud columns contain multi-layer clouds, with the majority of multi-layered cloud columns containing two cloud layers. According to the analysis of radiosonde soundings with 30 hPa or 50 hPa vertical resolutions, multilayer cloud systems occur in 56% or 28%, respectively, of the soundings containing any cloud layers (Fig. 18 of Wang and Rossow (1995)). Considering that the thickness of the ECMWF model levels is about 40 hPa in the mid-troposphere, the ECMWF model slightly underestimates the frequency of multilayer cloud systems.

Histograms of cloud thickness and separation distance are presented in Fig. A.2. Qualitatively, the shape of these histograms agrees well with the observations (Figs. 20 and 25, respectively, of Wang and Rossow (1995)). One important difference is that if one model level is assumed to be 500 m thick, the histogram of cloud thickness falls off more slowly than indicated by the observations; i.e. the ECMWF model has more cloud layers of moderate to large thickness than are observed. However, the thickness of cloud layers in the ECMWF model is sensitive to the threshold used to define cloud occurrence. If levels with cloud fractions less than 0.1 are excluded, the histogram of cloud thickness falls off more rapidly. The abundance of cloud fractions less than 0.1 in levels next to those with cloud fractions greater than 0.1 has been found to be related to vertical advection of cloud fraction by the mean wind.

Statistics of cloud vertical structure resolved by the subgrid model (see Fig. 4) are similar to those presented above.

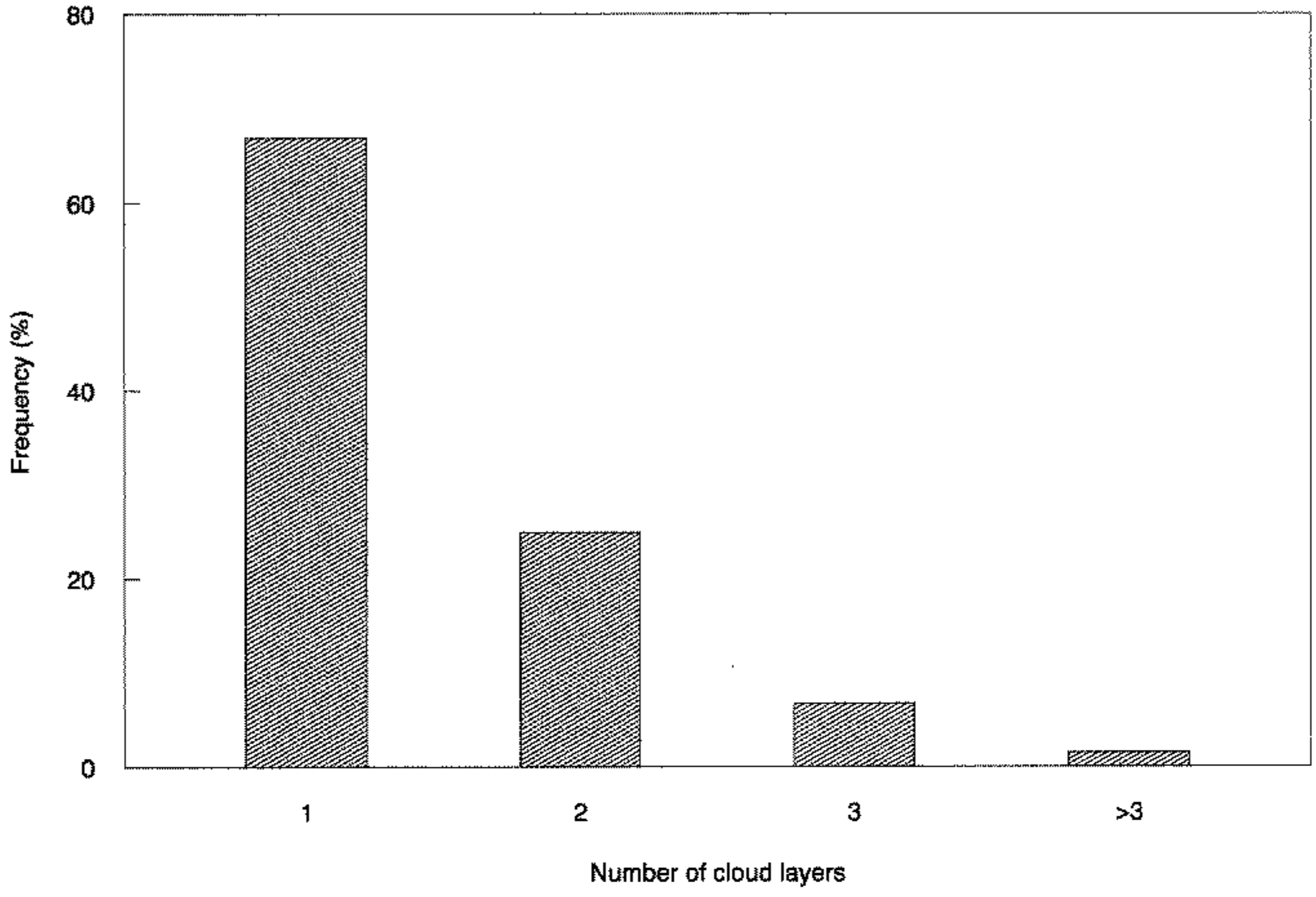

Figure A.1. Frequency distribution of the number of cloud layers in a T63L31 24-hour forecast.

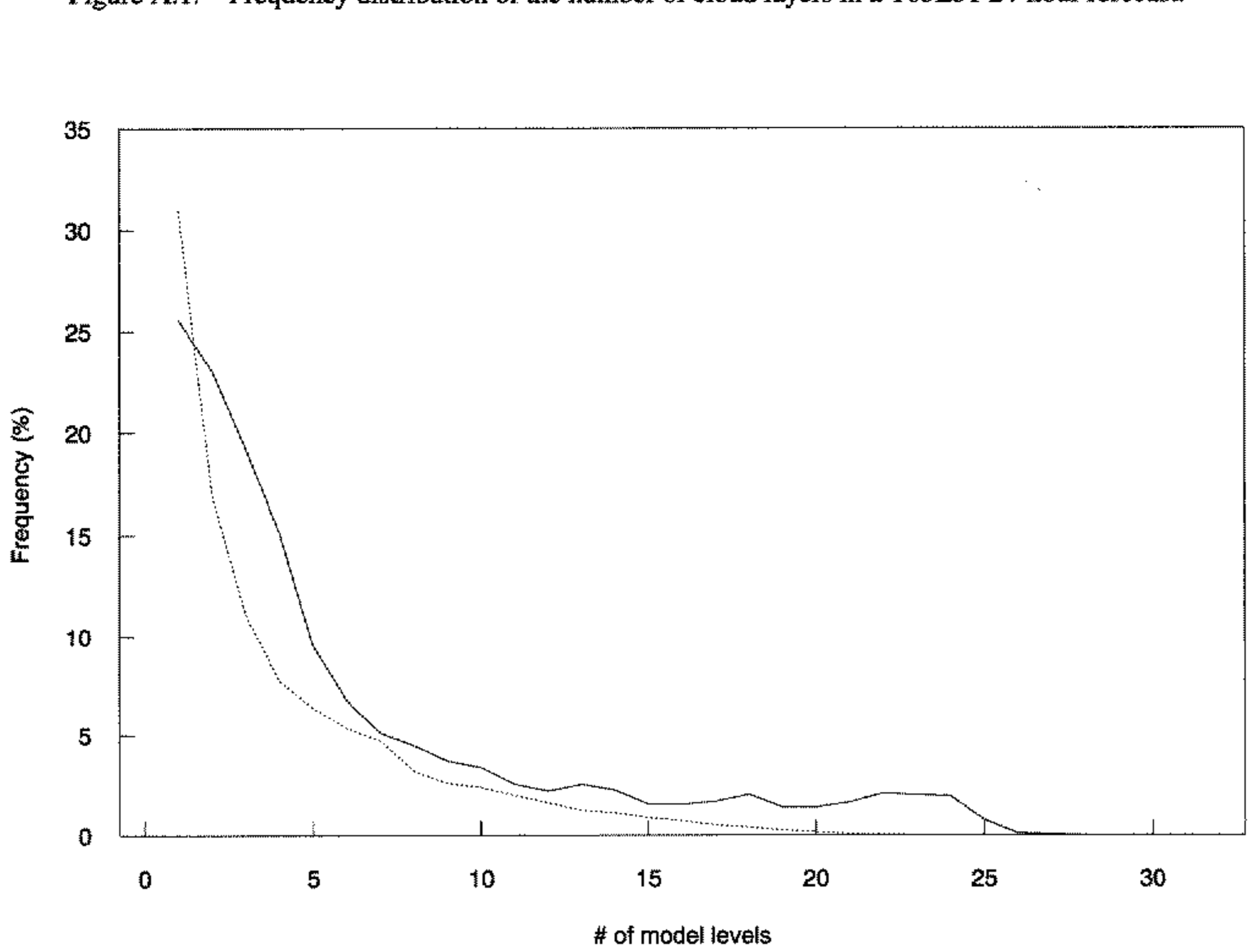

Figure A.2. Frequency distribution of the thickness (full line) and separation distance (dotted line) of cloud layers in a T63L31 24-hour forecast.

REFERENCES

Baker, M. B. 1997 Cloud microphysics and climate. *Science*, **276**, 1072–1078

Bechthold, P., Pinty, J. P. and Mascart, P. 1993 The use of partial cloudiness in a warm-rain parameterization: A subgrid-scale precipitation scheme. *Mon. Weather Rev.*, **121**, 3301–3311

Del Genio, A. D., Yao, M.-S., Kovari, W. and Lo, K. K.-W. 1996 A prognostic cloud water parametrization for global climate models. *J. Climate*, **9**, 270–304

Fowler, L. D., Randall, D. A. and Rutledge, S. A. 1996 Liquid and ice cloud microphysics in the CSU general circulation model. Part I: Model description and simulated microphysical processes. *J. Climate*, **9**, 489–529

Geleyn, J.-F. and Hollingsworth, A. 1979 An economical analytical method for the computation of the interaction between scattering and line absorption of radiation. *Beitr. Phys. Atmos.*, **52**, 1–16

Gregory, D. 1995 A consistent treatment of evaporation of rain and snow for use in large-scale models. *Mon. Weather Rev.*, **123**, 2716–2732

Heymsfield, A. J. and Donner, L. J. 1990 A scheme for parameterizing ice-cloud water content in general circulation models. *J. Atmos. Sci.*, **47**, 1865–1877

Houze, R. A. and Betts, A. K. 1981 Convection in GATE. *Rev. Geophys. Space Phys.*, **19**, 541–576

Hsie, E. Y., Farley, R. D. and Orville, H. D. 1980 Numerical simulation of ice phase convective cloud seeding. *J. Appl. Meteorol.*, **19**, 950–977

Jakob, C. 1994 'The impact of the new cloud scheme on ECMWF's integrated forecasting system (IFS)'. In Proceedings of the ECMWF/GEWEX workshop on modelling, validation and assimilation of clouds, November 1994, European Centre for Medium-Range Weather Forecasts, Shinfield Park, Reading, RG2 9AX, UK

Kessler, E. 1969 On the distribution and continuity of water substance in atmospheric circulations. *Meteorol. Monogr.*, **10**, 32, American Meteorological Society, Boston, USA

Liang, X.-Z. and Wang, W.-C. 1997 Cloud overlap effects on general circulation model climate simulations. *J. Geophys. Res.*, **102**, 11039–11047

Lin, Y.-L., Farley, R. D. and Orville, H. D. 1983 Bulk-parameterization of the snow field in a cloud model. *J. Climate Appl. Meteorol.*, **22**, 1065–1092

Mace, G. G., Jakob, C. and Moran, K. P. 1998 Validation of hydrometeor occurrence predicted by ECMWF model using millimeter wave radar data. *Geophys. Res. Letters*, **25**, 1645–1648

Morcrette, J.-J. and Fouquart, Y. 1986 The overlapping of cloud layers in shortwave radiation parameterizations. *J. Atmos. Sci.*, **43**, 321–328

Rotstayn, L. D. 1997 A physically based scheme for the treatment of stratiform clouds and precipitation in large-scale models. I: Description and evaluation of the microphysical processes. *Q. J. R. Meteorol. Soc.*, **123**, 1227–1282

Rutledge, S. A. and Hobbs, P. V. 1983 The mesoscale and microscale structure and organization of clouds and precipitation in midlatitude cyclones. VIII: A model for the 'seeder–feeder' process in warm-frontal rainbands. *J. Atmos. Sci.*, **40**, 1185–1206

Smith, R. N. B. 1990 A scheme for predicting layer clouds and their water content in a general circulation model. *Q. J. R. Meteorol. Soc.*, **116**, 435–460

Stubenrauch, C. J., Del Genio, A. D. and Rossow, W. B. 1997 Implementation of subgrid cloud vertical structure inside a GCM and its effect on the radiation budget. *J. Climate*, **10**, 273–287

Sui, C.-H., Lau, K.-M., Takayabu, Y. N. and Short, D. A. 1997 Diurnal variations in tropical oceanic cumulus convection during TOGA COARE. *J. Atmos. Sci.*, **54**, 639–655

Sundqvist, H. 1978 A parameterization scheme for non-convective condensation including prediction of cloud water content, *Q. J. R. Meteorol. Soc.*, **104**, 677–690

Sundqvist, H. 1988 'Parameterization of condensation and associated clouds in models for weather prediction and general circulation simulation'. Pp. 433–461 in *Physically-Based Modelling and Simulation of Climate and Climate Change*, Ed. M.E. Schlesinger, Kluwer

Tian, L. and Curry, J. A. 1989 Cloud overlap statistics. *J. Geophys. Res.*, **94**, 9925–9935

Tiedtke, M. 1993 Representation of clouds in large-scale models, *Mon. Weather Rev.*, **121**, 3040–3061

Tiedtke, M. 1996 An extension of cloud-radiation parameterization in the ECMWF model: The representation of subgrid-scale variations of optical depth. *Mon. Weather Rev.*, **124**, 745–750

Wang, J. and Rossow, W. B. 1995 Determination of cloud vertical structure from upper-air observations. *J. Appl. Meteorol.*, **34**, 2243–2258

Yu, W., Doutriaux, M., Sèze, G., LeTreut, H. and Desbois, M. 1996 A methodology study of the validation of clouds in GCMs using ISCCP satellite observations. *Climate Dyn.*, **12**, 389–401